JGR Planets

RESEARCH ARTICLE
10.1029/2022JE007455

Special Section:
The Mars Perseverance Rover Jezero Crater Floor Campaign

SHERLOC Raman Mineral Class Detections of the Mars 2020 Crater Floor Campaign

Andrea Corpolongo[1], Ryan S. Jakubek[2], Aaron S. Burton[3], Adrian J. Brown[4], Anastasia Yanchilina[5], Andrew D. Czaja[1], Andrew Steele[6], Brittan V. Wogsland[7], Carina Lee[8], David Flannery[9], Desirée Baker[1], Edward A. Cloutis[10], Emily Cardarelli[4], Eva L. Scheller[11], Eve L. Berger[12], Francis M. McCubbin[3], Joseph Razzell Hollis[4], Keyron Hickman-Lewis[13,14], Kim Steadman[4], Kyle Uckert[4], Lauren DeFlores[4], Linda Kah[7], Luther W. Beegle[15], Marc Fries[3], Michelle Minitti[16], Nikole C. Haney[2], Pamela Conrad[6], Richard V. Morris[3], Rohit Bhartia[17], Ryan Roppel[18], Sandra Siljeström[19], Sanford A. Asher[18], Sergei V. Bykov[18], Sunanda Sharma[4], Svetlana Shkolyar[20,21,22], Teresa Fornaro[23], and William Abbey[4]

[1]Department of Geology, University of Cincinnati, Cincinnati, OH, USA, [2]Jacobs, NASA Johnson Space Center, Houston, TX, USA, [3]NASA Johnson Space Center, Houston, TX, USA, [4]Jet Propulsion Laboratory, California Institution of Technology, Pasadena, CA, USA, [5]Impossible Sensing Incorporated, St. Louis, MO, USA, [6]Carnegie Institute of Washington, Washington, DC, USA, [7]Department of Earth and Planetary Sciences, University of Tennessee, Knoxville, TN, USA, [8]Lunar & Planetary Institute, Universities Space Research Association, Houston, TX, USA, [9]Queensland University of Technology, Brisbane, QLD, Australia, [10]Department of Geography, University of Winnipeg, Winnipeg, MB, Canada, [11]California Institute of Technology, Pasadena, CA, USA, [12]Texas State University, Jacobs JETS, NASA Johnson Space Center, Houston, TX, USA, [13]The Natural History Museum, London, UK, [14]Dipartimento BiGeA, Università di Bologna, Bologna, Italy, [15]Formerly at Jet Propulsion Laboratory, California Institution of Technology, Pasadena, CA, USA, [16]Framework, Silver Spring, MD, USA, [17]Photon Systems Incorporated, Covina, CA, USA, [18]Department of Chemistry, University of Pittsburgh, Pittsburgh, PA, USA, [19]RISE Research Institutes of Sweden, Stockholm, Sweden, [20]USRA, Columbia, MD, USA, [21]NASA Goddard Space Flight Center, Greenbelt, MD, USA, [22]Blue Marble Space Institute of Science, Seattle, WA, USA, [23]INAF-Astrophysical Observatory of Arcetri, Florence, Italy

Abstract The goals of NASA's Mars 2020 mission include searching for evidence of ancient life on Mars, studying the geology of Jezero crater, understanding Mars' current and past climate, and preparing for human exploration of Mars. During the mission's first science campaign, the Perseverance rover's SHERLOC deep UV Raman and fluorescence instrument collected microscale, two-dimensional Raman and fluorescence images on 10 natural (unabraded) and abraded targets on two different Jezero crater floor units: Séítah and Máaz. We report SHERLOC Raman measurements collected during the Crater Floor Campaign and discuss their implications regarding the origin and history of Séítah and Máaz. The data support the conclusion that Séítah and Máaz are mineralogically distinct igneous units with complex aqueous alteration histories and suggest that the Jezero crater floor once hosted an environment capable of supporting microbial life and preserving evidence of that life, if it existed.

Plain Language Summary The goals of NASA's Mars 2020 mission include searching for evidence of ancient life on Mars, studying the geology of Jezero crater, understanding Mars' current and past climate, and preparing for human exploration of Mars. During the mission's first science campaign, SHERLOC (Scanning Habitable Environments with Raman and Luminescence for Organics and Chemicals), one of Perseverance rover's spectroscopic instruments, collected microscale, two-dimensional images that displayed mineral and organic molecule detections on 10 natural (unabraded) and abraded targets on two different Jezero crater floor geological units: Séítah and Máaz. We report SHERLOC mineral detections made during the Crater Floor Campaign and discuss their implications regarding the origin and history of Séítah and Máaz. The mineral detections support the conclusion that Séítah and Máaz are igneous units with different mineral compositions and distinct histories of alteration by fluids. The detections further suggest that the Jezero crater floor was once home to an environment capable of supporting microbial life and preserving evidence of that life, if it ever existed.

The Mars Perseverance Rover Jezero Crater Floor Campaign

Andrea Corpolongo and Ryan S. Jakubek contributed equally to this work.

Key Points:

- The floor of the Jezero crater hosts distinct igneous units with differing aqueous alteration histories
- SHERLOC Raman mineral class detections indicate that the Jezero crater floor was once a habitable environment
- Some Crater Floor Campaign samples may contain salts known to preserve biosignatures in terrestrial analog environments

Supporting Information:

Supporting Information may be found in the online version of this article.

Correspondence to:

A. Corpolongo,
corpolaa@mail.uc.edu

Citation:

Corpolongo, A., Jakubek, R. S., Burton, A. S., Brown, A. J., Yanchilina, A., Czaja, A. D., et al. (2023). SHERLOC Raman mineral class detections of the Mars 2020 Crater Floor Campaign. *Journal of Geophysical Research: Planets*, *128*, e2022JE007455. https://doi.org/10.1029/2022JE007455

Received 30 JUN 2022
Accepted 17 JAN 2023

Author Contributions:

Conceptualization: Aaron S. Burton, Andrew Steele, Edward A. Cloutis, Luther W. Beegle, Marc Fries, Pamela Conrad, Rohit Bhartia, Sanford A. Asher, William Abbey
Data curation: Ryan S. Jakubek, Kyle Uckert, Rohit Bhartia
Formal analysis: Andrea Corpolongo, Ryan S. Jakubek, Anastasia Yanchilina, Eva L. Scheller, Joseph Razzell Hollis, Richard V. Morris, Ryan Roppel, Sunanda Sharma
Investigation: Andrea Corpolongo, Aaron S. Burton, Adrian J. Brown, Anastasia Yanchilina, Andrew D. Czaja, Andrew Steele, Brittan V. Wogsland, Carina Lee, David Flannery, Emily Cardarelli, Eva L. Scheller, Eve L. Berger, Joseph Razzell Hollis, Keyron Hickman-Lewis, Kim Steadman, Kyle Uckert, Lauren DeFlores, Linda Kah, Luther W. Beegle, Marc Fries, Michelle Minitti, Nikole C. Haney, Pamela Conrad, Rohit Bhartia, Ryan Roppel, Sandra Siljeström, Sanford A. Asher, Sergei V. Bykov, Sunanda Sharma, Svetlana Shkolyar, Teresa Fornaro, William Abbey
Project Administration: Luther W. Beegle, Rohit Bhartia
Software: Kyle Uckert
Supervision: Andrew Steele, Luther W. Beegle
Validation: Ryan S. Jakubek, Francis M. McCubbin, Joseph Razzell Hollis, Richard V. Morris
Visualization: Andrea Corpolongo, Andrew D. Czaja, Eve L. Berger
Writing – original draft: Andrea Corpolongo, Ryan S. Jakubek, Adrian J. Brown, Anastasia Yanchilina, Desirée Baker
Writing – review & editing: Andrea Corpolongo, Ryan S. Jakubek, Aaron S. Burton, Adrian J. Brown, Anastasia Yanchilina, Andrew D. Czaja, Andrew Steele, Brittan V. Wogsland, Emily Cardarelli, Eva L. Scheller, Eve L. Berger, Francis M. McCubbin, Keyron Hickman-Lewis, Linda Kah, Marc Fries, Michelle Minitti, Nikole C. Haney, Pamela Conrad, Richard V. Morris, Rohit Bhartia, Ryan Roppel, Sandra Siljeström, Sunanda Sharma, Svetlana Shkolyar, Teresa Fornaro, William Abbey

1. Introduction

On 18 February 2021, NASA's Mars 2020 mission Perseverance rover began exploring Jezero crater with the primary goal of searching for evidence of ancient life on Mars. Other goals include studying the geology of the region, understanding Mars' current and past climate, and preparing for human exploration (Farley et al., 2020). These goals are being addressed through in situ analyses by the rover's instruments and collection of a suite of compelling samples to be returned to Earth by future Mars Sample Return (MSR) missions.

The first campaign of the Mars 2020 mission was an exploration of the floor of Jezero crater (Sun et al., 2022; Figure 1). During this campaign, the rover investigated two major units, Séítah and Máaz, on the floor of Jezero crater that had been identified from orbital data before surface operations commenced (Stack et al., 2020). (Note that special characters and accents in target, rock, and unit names are omitted in many Mars 2020 documents because they cannot be included in the code used to communicate with Perseverance. As a result, alternate spellings, such as , Seitah, Maaz, and Chal, are often used for features with accents or special characters in their names.) The older unit, Séítah, previously referred to as the Crater Floor Fractured 1 (CF-F-1) Unit, is light-toned, ridged, and fractured. Séítah is overlain by Máaz, previously referred to as the Crater Floor Fractured Rough (CF-Fr) Unit, which is light-toned and polygonally fractured. Results from the Perseverance payload during the Crater Floor Campaign indicate that both Máaz and Séítah are igneous in origin (Horgan et al., 2022). Máaz is characterized by the presence of abundant pyroxene (Schmidt et al., 2022; Udry et al., 2022), while Séítah is an olivine cumulate (Brown et al., 2022: Farley et al., 2022; Liu et al., 2022; Núñez et al., 2022; Wiens et al., 2022). The transition between the Séítah and Máaz units is highlighted in cyan in Figure 1. The contact between the two units is obscured by regolith and not observable, however Séítah and Máaz vary in elevation by approximately 10 m along Artuby ridge (Figure 1), a resistant feature along the southern margin of the portion of the Séítah unit that Perseverance explored (Sun et al., 2022).

The Crater Floor Campaign addressed several objectives of the Mars 2020 mission by contributing to a scientific understanding of the geology of Jezero crater, seeking rocks with high probability of preserving ancient biosignatures and looking for potential biosignatures within rocks of the Séítah and Máaz units, and documenting the geological context of the first set of samples collected for possible future return to Earth. This paper reports spectral maps collected by SHERLOC (Scanning Habitable Environments with Raman and Luminescence for Organics and Chemicals), an arm mounted deep UV (DUV) Raman spectrometer (Bhartia et al., 2021). The maps are paired with high resolution (10.1 μm/pixel) grayscale images collected by the co-boresighted Autofocus Contex Imager (ACI), enabling mapping of the location where each Raman spectrum was collected on the target surface. In addition, the Wide Angle Topographic Sensor for Operations and eNgineering camera (WATSON) provides macro-scale, color images of the Raman scan targets. Combining the image color of WATSON images with the high resolution of the ACI images produces colorized ACI images that allow for the identification of individual mineral grains and the detection of associations between minerals and any detected organic matter. These capabilities make SHERLOC and WATSON of central importance in achieving the geological and astrobiological objectives of the Mars 2020 mission.

2. Methods

SHERLOC is a deep UV (DUV) Raman and fluorescence spectrometer designed to detect, characterize, and spatially resolve organics and minerals on the Martian surface (Bhartia et al., 2021). A 248.6 nm DUV laser is used for excitation and takes advantage of increased scattering Raman cross section from Rayleigh Law and resonance enhancement, allowing for the detection of small quantities of organics and minerals. Many molecules, when excited, fluoresce at wavelengths above ~270 nm, at intensities many orders of magnitude greater than the intensities of typical Raman peaks, making it difficult to impossible to detect any Raman scattering that might coincide with such strong fluorescence bands. Unlike longer wavelength lasers (near-UV, visible, or near IR), the DUV Raman spectral window is energetically separated from the fluorescence window, allowing for Raman and fluorescence spectra to be obtained in non-overlapping spectral regions (Bhartia et al., 2012; Eshelman et al., 2014; Montagnac et al., 2021; Tarcea et al., 2007). The depth of field of the SHERLOC instrument is ±500 μm to accommodate the surface roughness of the abraded patch; however, it is expected that the Raman response is coming from a 100–200 μm depth of penetration (Bhartia et al., 2021; Carrier et al., 2019). The DUV laser-injection filter optical coating attenuates <800 cm^{-1}, limiting the detection of primary Raman bands of many silicates and oxides. In addition, DUV absorbing minerals (i.e., some Fe containing minerals) can attenuate the depth of penetration into a material and reduce the signal to noise ratios (SNR) (Morris et al., 2022; Razzell Hollis, Abbey, et al., 2021).

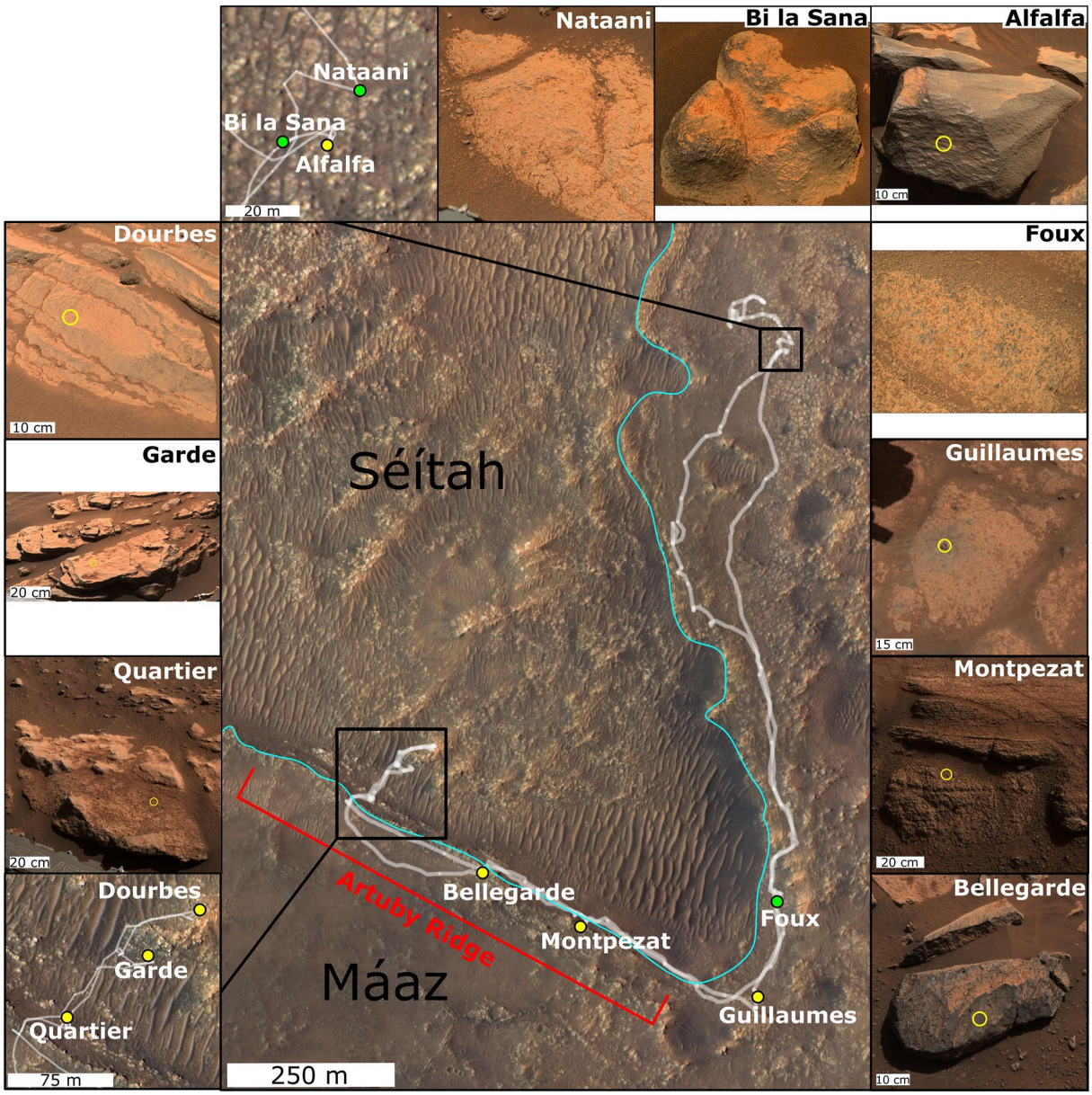

Figure 1. A map of the Crater Floor Campaign traverse (central image and insets, based on HiRISE imagery) and natural and abraded targets analyzed by proximity science, including SHERLOC and WATSON, through sol 370 (smaller images around the periphery, imaged by the MastCam-Z instrument on the Perseverance rover). The white path on the map shows Perseverance's traverse. The cyan line marks the approximate contact between the Séítah formation below and the Máaz formation above. The red bracket indicates the Artuby Ridge. Targets analyzed are indicated along the route. The yellow circles on most targets indicate the location of the abrasion patches (see subsequent figures). Those without yellow circles were not abraded.

SHERLOC is an arm-mounted instrument, which allows it to be moved into the proximity of an analysis target. With no change in arm position, an internal scanning mirror rasters the deep UV laser beam across the sample surface. With a maximum area of 7 mm × 7 mm, Raman/fluorescence spectra are acquired at discrete points with a beam diameter of ∼100 μm (Bhartia et al., 2021). Prior to each spectral scan, the Autofocus Context Imager (ACI) was used to acquire 10.1 μm/pixel resolution grayscale images of the target surface. This provides context for the spectral maps and is used to focus the spectrometer/laser. Color images acquired by WATSON have a spatial resolution ranging from 16 to 150 μm/pixel and are used for targeting SHERLOC observations and textural analysis (Bhartia et al., 2021; Edgett et al., 2012). SHERLOC is designed to simultaneously collect Raman and fluorescence data on the same CCD with a single readout. To reduce noise, the CCD readout is binned into three regions, a Raman region

~800–4000 cm^{-1} (250–273 nm) and two fluorescence regions (274–337 and 338 to ~370 nm). Each region has a separate wavenumber calibration, previously discussed in detail (Uckert et al., 2021).

2.1. Scan Procedures

In this paper, we use the following nomenclature to describe SHERLOC Raman measurements (Figure S1 in Supporting Information S1). A "target" refers to the specific rock or abraded patch on which data were collected, such as "Nataani" or "Guillaumes," while a "scan" refers to a specific Raman hyperspectral map that was collected on a target. Each Raman scan is named using the nomenclature "#0001_name_#2_#3," wherein #0001 denotes the sol on which the scan was performed, name refers to the target and describes the parameters of the scan, #2 is the laser pulses per each point spectrum within a scan, and #3 is the scan number used to differentiate between multiple scans of the same parameter made on the same sol. Each individual spectrum within a scan is referred to as a "point," and each point within a scan is assigned a number according to the order it occurred in the scan. The first Raman spectra collected within a scan falls at the upper left corner of the hyperspectral map. The collection continues in a serpentinite pattern, such that the final spectrum in a 100 point scan falls at the lower left corner of the map. High Dynamic Range (HDR) scans consist of 100 points with 780 μm spacing for an image size of 7 mm × 7 mm. Detail scans consist of 100 points with 100 μm spacing for an image size of 1 mm × 1 mm. Survey scans consist of 1,296 points with fixed spacing between them (50, 144, or 200 μm, depending on the scan template) and 10 or 15 pulses per point. For example, the scan name "0083_Nataani HDR_50_1" describes the first HDR scan performed on Nataani using 50 pulses per point on sol 83 of the Mars 2020 mission.

For each scan SHERLOC performs, single spectra are obtained by first collecting a dark spectrum with no incident laser light and then collecting the active spectrum with the laser firing. The dark scan is then subtracted from the active spectrum to produce the reported Raman spectrum. SHERLOC spectra have a ~10 cm^{-1}/pixel resolution with a Raman spectral range of ~800–4,000 cm^{-1}. The potential to observe Raman bands in the spectral range below 800 cm^{-1} is limited because SHERLOC's laser-injection filter has reduced transmission in this region and the 252.9 nm laser plasma line is observed at ~650 cm^{-1}. However, very strong bands below 800 cm^{-1} can be observed (Bhartia et al., 2021; Razzell Hollis, Abbey, et al., 2021; Uckert et al., 2021).

We performed scans on both natural and abraded targets. Targets were abraded using Perseverance's Rock Abrasion Tool (RAT), which is ~45 mm in diameter and capable of creating smooth-bottomed abraded patches up to ~1 cm deep. After abrasion, abraded patches are cleaned of dust and cuttings by the gaseous dust removal tool (gDRT), which blasts the abraded target with a high-velocity jet of nitrogen gas (Farley et al., 2020; Moeller et al., 2021). The targets described below as abraded targets were abraded and cleaned as described prior to scanning. Any targets described below as natural targets were neither abraded nor cleaned with the gDRT prior to scanning.

2.2. Data Analysis Procedures

We examined each individual Raman spectrum in each scan. We considered any band with a FWHM of 30 cm^{-1} (~3 pixels) or more a potential Raman signal. We assigned each single spectrum containing observable Raman signals to its respective mineral class via comparison to standard spectra obtained through laboratory measurements with the SHERLOC Brassboard instrument, an analog DUV Raman and fluorescence instrument housed at the NASA Jet Propulsion Laboratory (described in detail by Razzell Hollis, Abbey, et al. (2021) and Razzell Hollis, Ireland, et al. (2021)) and ACRONM (Analog Complementary Raman for Operations oN Mars) (see Text S4.1 in Supporting Information S1 for a discussion of SHERLOC analog instruments). All peak centers were determined by a Gaussian fit function, through the open-source peak fitting software Fityk (version 1.3.1; Wojdyr, 2010).

In Section 3, we display the SHERLOC Raman data through Raman spectral assignments overlain on each scan's associated ACI image. These spectral assignment maps are accompanied by colorized ACI images overlaid with white rings that indicate the location of each point in the scan. The spectral positioning calculations were validated from images of ACI calibration measurements where dust mobilization could be observed. Spectral map/ACI overlays are accurate to within ~44 μm near the center of maps, and within 115 μm at the 7 mm × 7 mm map corners in the HDR overlays. The points at the start of each scan (scans start at the upper left corner) have less location uncertainty than points at the end of the map scan because of robotic arm drift, which can add up to ~30 μm of uncertainty. Each laser shot hits the scanned surface as an annulus ~100 μm in diameter. The white rings overlying the colorized ACI images are ~200 μm in diameter so that the location being analyzed is visible.

We used Bayer-encoded 8-bit WATSON color and grayscale ACI image products for this study to most closely represent the raw data from the image detector. To generate secondary image products, we performed further processing on both WATSON and ACI products using a custom Python script to register multiple images for a single target to create an overlay. ACI companded image products and WATSON companded or companded *z*-stack range images (~4–10 cm standoff) images were used in all cases. "Colorized" ACI images used for correlating spectral, color, and textural information were generated as previously described (Scheller et al., 2022).

2.3. Spectra Signal-To-Noise Analysis

In order to quantitatively assign confidence in SHERLOC mineral detections, we developed a statistical procedure involving comparing apparent signal intensities to a calculated median root-mean-squared-deviation (RMSD) of the noise for each scan. We first calculated the noise RMSD in the 2500–3000 cm^{-1} region of Raman spectra for every individual spectrum in each scan. This "silent" region was selected for its lack of signal in any spectrum, excluding cosmic ray artifacts. Then, we determined the median of the noise RMSD values for each scan. We used the median to avoid contributions from any RMSD values that were inflated by cosmic rays, background fluorescence, and other spectral effects. The RMSD noise values differed between Raman images but generally occur in the 20–50 count range.

We designated single spectra Raman bands with intensities ≥3X the noise RMSD as statistically significant signals. This designation criterion is based on the International Union of Pure and Applied Chemistry's limit of detection for the probability of a data point being statistically above a normally distributed noise background (McNaught & Wilkinson, 1997). The peak position error for SHERLOC Raman bands with intensities ≥3X the noise RMSD is ≤±~4.0 cm^{-1}. We used mean spectra to assign detections to mineral classes. By doing so, we obtained spectra with maximum peak intensities ≥10X the noise RMSD, which have a peak position error of <±~1 cm^{-1}. Combined with the ±1.8 cm^{-1} uncertainty in the wavenumber calibration (Fries et al., 2022), the peak wavenumber error of the most intense peaks in spectra used to assign mineral classes is approximately ±2-3 cm^{-1}. However, the error for any specific peak in a single spectrum is dependent on the signal-to-noise ratio and can be estimated using the work of Lenz and Ayres (1992), as described in Text S1 of Supporting Information S1. In the main text, the peak wavenumber values reported are approximate values for a mineral class assignment and are only meant to qualitatively describe the spectra for discussion. As described in Supporting Information S1, most mineral class assignments were assigned based on multiple Raman bands, and for mineral classes where only one band is present (carbonate, pyroxene, and silicate), the bands have distinctive Raman shifts. Thus, the mineral class assignments are not peak wavenumber error limited.

In the context of this paper, signals with ≥3X the noise RMSD are qualitatively observed with high confidence while those <3X are observed with less confidence. For these reasons, in the ACI-Raman image overlay figures presented in Section 3, we differentiate between Raman signals ≥3X and <3X the RMSD noise as a first-order indicator of the assignment confidence. To make this distinction, we label assignments made based on Raman signals ≥3X the noise with capital letters and those made based on signals <3X the noise with lowercase letters. In the text, we describe assignments made based on Raman signals ≥3X the noise as definitive and assignments made based on signals <3X the noise as probable or possible.

2.4. Background Spectral Features

It is important to note several spectral features observed as background in SHERLOC Raman spectra. These features are characterized by Raman scans collected with no target at the laser focus, referred to as the stowed arm scans. We collected HDR_100, _250, and _500 scans with SHERLOC in the stowed position. We detected a weak Raman peak of fused silica that originated from Raman scattering of the instrument optics, seen as broad peaks at ~480 cm^{-1} and ~800 cm^{-1} (Text S2 in Supporting Information S1). This background feature is of sufficiently weak intensity that it is observed only in spectra with ≥500 pulses/point. In addition, the fused silica background is distinct from all Raman signals obtained from sample targets and does not interfere with spectral analysis.

We also observed narrow peaks occurring at specific wavenumbers more frequently than would be expected if they were occurring randomly. These peaks are artifacts of the dark spectrum subtraction process described in Section 2.1. Most of the artifact peaks occur at wavenumbers that are irrelevant to the spectral assignments in this paper. However, we observed narrow peaks at 970 cm^{-1} and/or 981 cm^{-1} in ~20% of the stowed arm spectra, which increases the uncertainty of spectral assignments relying on peaks at or near these wavenumbers. At the

time of writing, the SHERLOC team is working to determine the cause and mitigate the influence of these artifacts. See Text S3 in Supporting Information S1 for a detailed discussion of this topic.

3. Results

SHERLOC scanned 10 targets during the Crater Floor Campaign: three from Séítah (all abraded surfaces) and seven from Máaz (three natural and four abraded surfaces) (Figure 1). SHERLOC successfully performed within operating capabilities on Mars, becoming the first Raman spectrometer to map the mineral composition in context on the surface of another planetary body.

In Sections 3.1 and 3.2, beginning with the stratigraphically lower Séítah targets and moving upsection to Máaz targets, we report the results of SHERLOC's microscale mineral mapping on the Jezero crater floor. For each target, we describe textural features of the scanned rock surfaces revealed by WATSON imagery, report mineral detections facilitated by SHERLOC Raman spectroscopy at each target, and highlight associations between textural features and mineral detections.

Mineral assignments reported below are to mineral class only and not to mineral species, with the exception of sodium perchlorate assignments reported in Section 3.2.1. Assignments include undefined silicate (labeled silicate throughout the text), carbonate, olivine, perchlorate/phosphate, perchlorate, sodium perchlorate, pyroxene, and sulfate. Class assignments were made by comparing fitted mean or individual SHERLOC spectra (as specified in the individual reports below) to standard spectra collected with the DUV SHERLOC analog instruments Brassboard and ACRONM, as shown in Figures 2–8.

Spectra assigned undefined silicate feature a broad band centered at ∼1050 cm^{-1} that is similar to broad bands between 900 and 1200 cm^{-1} observed in some silicate spectra collected on ACRONM. The bands are qualitatively similar to ACRONM spectra of plagioclase feldspar (Figures 2, 3, 6, 7, and 8). However, the identifying Raman peaks of feldspars (and many other silicates) occur below 800 cm^{-1}, in the spectral range that is obscured by SHERLOC's laser-injection filter and laser plasma line. Some of the broad bands centered at ∼1050 cm^{-1} could represent detections of amorphous silica, as amorphous silica would yield spectra with a similar feature (Fu et al., 2017). However, the broad nature of these bands is also similar to broad bands centered between 1000 and 1020 cm^{-1} in augite, labradorite, and bytownite spectra collected on Brassboard (Razzell Hollis, Abbey, et al., 2021), which further indicates that SHERLOC scans of crystalline silicates may yield broad spectral features. As a result, we cannot make more specific mineral assignments of spectra featuring broad bands centered at ∼1050 cm^{-1} at this time, as they may represent detections of crystalline or amorphous mineral phases. The SHERLOC team is actively working to determine exactly how the laser injection filter affects peak intensity and placement in the spectral range below 800 cm^{-1}. This work will be reported in a future publication. Unlike other silicates, the Raman spectra of olivine and pyroxene have identifying peaks above 800 cm^{-1}, allowing us to assign SHERLOC spectra to these mineral classes.

The dominant peaks in pyroxene and sulfate Raman spectra can fall within the same spectral range, of ∼970 cm^{-1} to 1050 cm^{-1} (e.g., Razzell Hollis, Abbey, et al., 2021). We differentiated between these assignments based on the presence of characteristic secondary peaks and hydration features in sulfate spectra, and by confirming pyroxene assignments with data collected by PIXL, Perseverance's micro-X-Ray fluorescence spectrometer, when possible. The dominant peaks of perchlorate and phosphate fall in a partially overlapping spectral range, between ∼950 cm^{-1} and 970 cm^{-1}. Where we observed peaks in this range, we distinguished between phosphate and perchlorate based on the presence of secondary perchlorate peaks. Where we observed peaks between ∼950 cm^{-1} and 970 cm^{-1} with no secondary peaks, we assigned spectra to perchlorate/phosphate. Criteria for all mineral assignments reported below are discussed in greater detail in Text S4 of Supporting Information S1.

3.1. Séítah Targets

3.1.1. Dourbes

The Dourbes abrasion, which was approximately 7 mm deep, was made on sol 251 on Brac, an outcrop of the Bastide member of the Séítah formation that featured centimeter to decimeter scale layering (Figure 1). The pre-abrasion surface of Brac was fluted from apparent wind abrasion and dust coated (Figure S2a in Supporting Information S1). The lowest relief areas of the surface of Brac were filled with coarse regolith and fine-grained

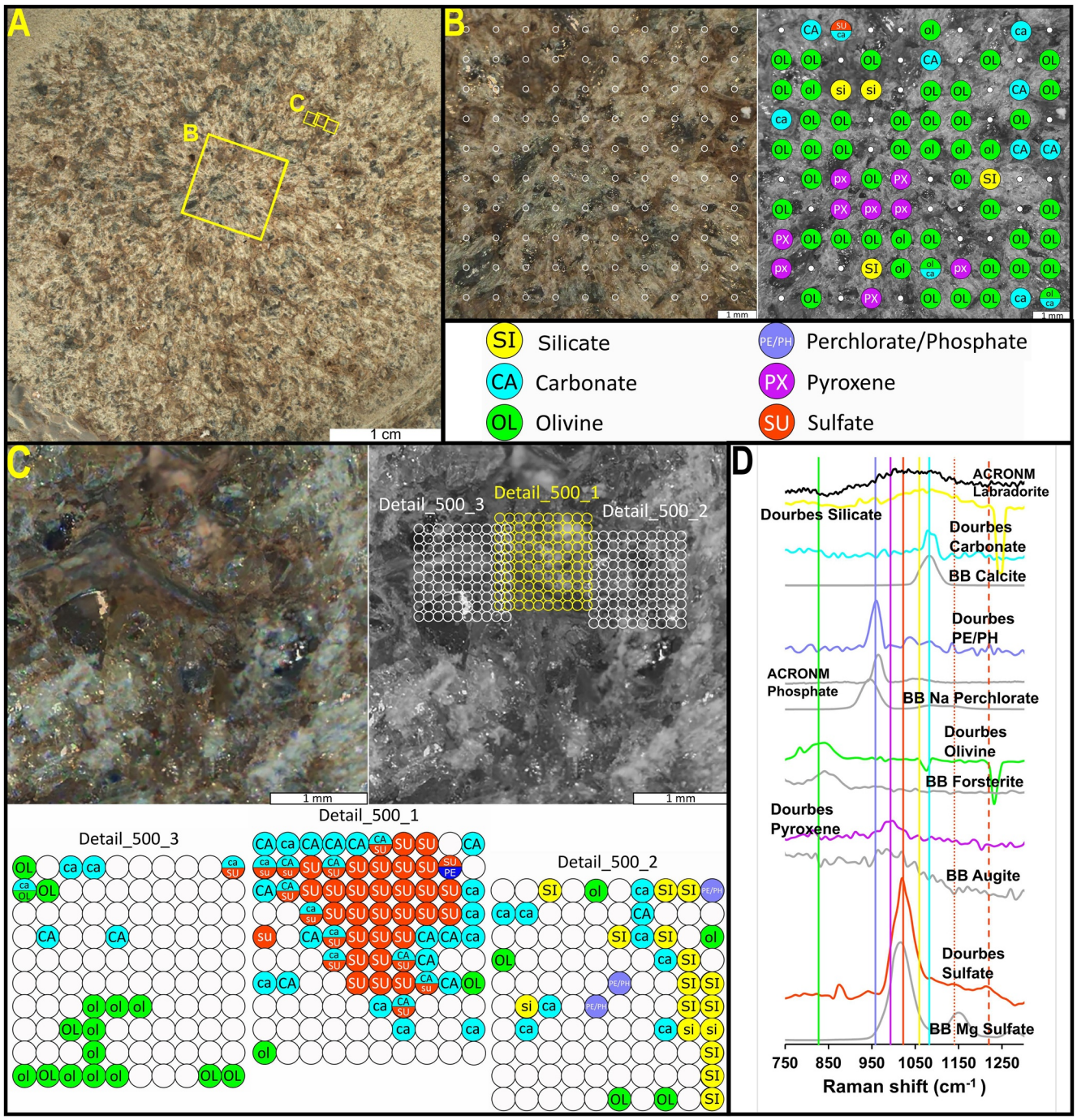

Figure 2. SHERLOC Raman mineral identifications from Dourbes. (a) The abrasion patch imaged by WATSON (image ID SI1_0257_0689775622_738FDR_N0080000SRLC00006_000095J01). Yellow boxes indicate the location of the scans performed. (b) Colorized (left) and grayscale (right) ACI images (image ID SC3_0257_0689786306_125FDR_N0080000SRLC11421_0000LMJ01) of the region of the abrasion patch bounded by the larger yellow box in panel (a). The white circles in panel B indicate the locations of SHERLOC analysis spots. Mineral identifications are indicated in the right panel. (c) Colorized (left) and grayscale (right) ACI images (image ID SC3_0269_0690851147_347FDR_N0080000SRLC11373_0000LMJ02) of the region of the abrasion patch bounded by the smaller yellow boxes in panel (a). The white and yellow circles in the upper right subpanel of panel C indicate the locations of SHERLOC analysis spots for three 1 mm^2 Detail scans. The lower three subpanels show mineral identifications for these three Detail scans. (d) Representative Raman spectra of minerals detected with high confidence from the abrasion patch and spectra of mineral standards collected on the SHERLOC Brassboard instrument at JPL and the ACRONM instrument at JSC. Vertical lines indicate peak centers. Spectra are offset along the *y*-axis for clarity.

gravel. Two core samples retrieved from Brac, Salette and Coulettes, are associated with the Dourbes abrasion (Simon et al., 2022). The abraded surface of Dourbes features ∼1–3 mm angular light gray-to-green and dark brown-to-black mineral grains (Figures 2a–2c). The gray-to-black grains are highly reflective. These grains are frequently rimmed by a light tan material and a reddish-brown material occurs in the spaces between them. The surface of Dourbes has no pitting or staining.

SHERLOC scans of Dourbes include 0257_Dourbes Survey_15_1, 0257_Dourbes HDR_500_1, 0269_Dourbes Survey_15_1, 0269_Dourbes Detail_500_1, 0269_Dourbes Detail_500_2, and 0269_Dourbes Detail_500_3 (Figure 2). The individual spectra from the Dourbes Survey scans contain no discernible peaks. The mean spectrum of each of these scans has a very weak possible silicate band (see Text S4.2 in Supporting Information S1), a weak possible O-H stretching band, and the background fused silica spectra discussed in Section 2.4 (Figure S1b in Supporting Information S1). The remaining scans contain spectra consistent with olivine, carbonate, pyroxene, sulfate, and perchlorate or phosphate in addition to silicate (Figures 2b–2d).

Olivine was the most common detection in 0257_Dourbes HDR_500_1 (Figure 2b). Thirty-eight percent of the points in this scan were definitively assigned to olivine and a further 8% were assigned as probable olivine. The dominant peak in the mean spectrum of all points in 0257_Dourbes HDR 500_1 definitively assigned to olivine is centered at 827 cm^{-1} (Figure 2d). The olivine standard spectrum in Figure 3d was collected with Brassboard from a natural forsterite sample (WARDS) and exhibits a primary peak centered at 844 cm^{-1}. Neither SHERLOC nor Brassboard has the spectral resolution required to resolve the doublet at ∼820 and ∼850 cm^{-1} that is typically observed in olivines and can be used to determine the olivine composition (Chopelas, 1991; Kuebler et al., 2006; Razzell Hollis, Abbey, et al., 2021). Correlating SHERLOC's unresolved olivine doublets to olivine Fo content is beyond the scope of this paper, as changes in the unresolved band position and width are controlled by the relative positions and intensities of the individual ∼820 and ∼850 cm^{-1} bands (see Text S4.3 in Supporting Information S1).

Carbonate and pyroxene were also prominent detections in this scan, with 5% of the points definitively assigned to carbonate, 6% assigned probable carbonate, 4% definitively assigned to pyroxene, and 5% assigned probable pyroxene. In addition, one point was definitively assigned to silicate and two were assigned as probable silicates. One point in this scan was definitively assigned to sulfate. The mean spectrum of all points in 0257_Dourbes HDR 500_1 definitively assigned to pyroxene is centered at 993 cm^{-1}, which is consistent with the augite spectrum collected by Brassboard (Figure 2d). The comparison to a standard augite spectrum is not a formal mineral species assignment, which will require a detailed investigation that is beyond the scope of this paper. This peak could also be consistent with hydrated sulfate species. We determined that the Dourbes points assigned to pyroxene are unlikely to be sulfate because they lack detectable hydration features and because PIXL, Perseverance's micro-X-Ray fluorescence spectrometer that provides spatially resolved elemental abundances, detected silicon, magnesium, and aluminum, but no sulfur, in the region of these detections, which is consistent with the presence of pyroxene (Razzell Hollis et al., 2022).

The three Dourbes Detail scans yielded sulfate, carbonate, olivine, silicate, perchlorate, and phosphate or perchlorate detections. Scan 0269_Dourbes Detail_500_1 is dominated by sulfate detections surrounded by carbonate detections, much like the larger carbonate rimmed sulfate in Quartier (Figure 4c; see Section 3.1.3). The dominant peak in the mean spectrum of all points in 0269_Dourbes Detail 500_1, assigned only to sulfate, is centered at 1022 cm^{-1}, represented by the vertical solid red line in Figure 2d. This mean spectrum also has weak secondary peaks at 1141 cm^{-1} and 1220 cm^{-1}, represented by the dotted and dashed vertical red lines in Figure 2d, and an OH stretching mode band (Figure S10b in Supporting Information S1). The primary peak in the Dourbes sulfate spectrum agrees closely with the primary peak of a synthetic magnesium sulfate (Macron Chemicals) spectrum collected on Brassboard, which is centered at 1019 cm^{-1} (Figure 4d). The secondary peaks of the Brassboard magnesium sulfate spectrum are at 1150 cm^{-1} and 1274 cm^{-1}. While these peaks do not correspond directly to the secondary peaks in the Dourbes sulfate spectrum, the secondary peaks of magnesium sulfate are reported to vary between ∼1060 cm^{-1} and ∼1260 cm^{-1}, depending on the hydration state of the mineral (Wang et al., 2006). The sulfate detections are concentrated on a sub-millimeter light brown to white grain (Figures 2c and 9b).

The single definitive perchlorate or chlorate detection in Dourbes is at point 11 of scan 0269_Dourbes Detail_500_1 (Figure 2c and Figure S12 in Supporting Information S1). This detection co-occurs with definitive sulfate detection and falls at the edge of the light brown to white sulfate grain, adjacent to carbonate detections.

We made this perchlorate assignment based on the presence of a peak at 932 cm^{-1}, which is consistent with the primary peak of several different perchlorate and chlorate species (see Text S4.8 in Supporting Information S1).

The dominant peak in the mean spectrum of all points in 0269_Dourbes Detail 500_1 assigned to carbonate is centered at 1083 cm^{-1}, represented by the vertical cyan line in Figure 2d. This peak corresponds closely to the 1084 cm^{-1} peak in the Brassboard terrestrial calcite standard spectrum (WARDS #49–5860) (Figure 2). The similarity between these spectra could suggest that the Dourbes carbonates are primarily calcite (see Text S4.4 in Supporting Information S1). However, this comparison is made with a mean spectrum of all carbonate points in the scan, so it is likely that carbonates with different cations contribute to the average peak position. Furthermore, minerals containing iron cations can absorb DUV laser radiation (Morris et al., 2022; Razzell Hollis, Abbey, et al., 2021; Razzell Hollis, Ireland, et al., 2021). This effect would have interfered with data acquisition if any of the detected carbonates contained iron. Therefore, we cannot assign SHERLOC carbonate detections to specific mineral species. The carbonate detections correspond to reddish-brown grains, primarily at the edge of the sulfate grain.

Scan 0269_Dourbes Detail_500_2 is the only SHERLOC scan of the Séítah formation in which the most common mineral detection is silicate. It also features olivine, carbonate, and perchlorate or phosphate detections. The band in the mean spectrum of all points in 0269_Dourbes Detail 500_1 assigned to silicate is centered at 1065 cm^{-1} and has a FWHM of 180 cm^{-1} (Figure 2d). This mean spectrum is similar to a labradorite spectrum standard collected with ACRONM. However, this similarity is not sufficient to assign the Dourbes silicate spectra to labradorite (Figure 2d). The silicate detections correspond to micron scale light gray-to-blue mineral grains. See Text S4.2 in Supporting Information S1 for additional details regarding silicate detections during the Crater Floor Campaign.

The perchlorate or phosphate peak in the mean spectrum of the three perchlorate or phosphate spectra in 0269_Dourbes Detail_500_2 is centered at ~958 cm^{-1} (Figure 4d). This falls between the dominant peak of a sodium perchlorate standard spectrum (collected with Brassboard from a sample of synthetic sodium perchlorate hydrate powder, Sigma Aldrich 310514) and that of a series of 11 natural and synthetic phosphate standards (collected with ACRONM and includes the minerals fluorapatite, hydroxylapatite, chlorapatite, whitlockite, and merrillite), which makes a confident mineral assignment difficult (Figure 2d). We observed no hydration features in the Dourbes perchlorate/phosphate spectra. The assignment of SHERLOC Raman peaks between ~950 cm^{-1} and 990 cm^{-1} is further complicated by the presence of relatively frequent artifacts at 970 cm^{-1} and 981 cm^{-1} in SHERLOC scans (see Section 2.4 and Text S3 in Supporting Information S1). These artifacts are easily identified when they occur in the absence of Raman signal. However, if they occur in a spectrum with a Raman signal between ~950 cm^{-1} and 990 cm^{-1}, they may artificially shift the center of the Raman peak.

Scan 0269_Dourbes Detail_500_3 detected olivine, carbonate, and, at a single point that overlaps with 0269_Dourbes Detail_500_1, sulfate. The dominant peak in the mean spectrum of all points in 0269_Dourbes Detail 500_3 assigned to olivine only is centered at 834 cm^{-1}. The olivine detections in the lower left corner of this scan correspond to a relatively large reflective dark brown-to-black euhedral mineral crystal and are not directly associated with carbonate detections (Figure 2c). Olivine detections in the upper left corner of this scan fall on a smaller subhedral black mineral crystal and are adjacent to carbonate detections that fall on a light reddish-brown grain (Figure 2c).

3.1.2. Garde

The abrasion patch Garde, which was approximately 11 mm deep, was made on sol 206 on the upper surface of a platy layered outcrop of the Bastide member of the Séítah formation called Bastide (Figure 1). The Bastide member is characterized by pronounced tabular layering, with most layers 1–3 cm thick and some 10–40 cm thick layers (Farley et al., 2022). The pre-abrasion surface of Garde was dust-coated, with occasional 2–3 mm, angular, elongate, gray-to-green mineral grains visible through the dust (Figure S2b in Supporting Information S1). Similar grains were recognized in SuperCam RMI images of relatively fresh outcrop surfaces and identified as olivine (Farley et al., 2022). The surface also exhibited infrequent millimeter scale pitting. No coring was attempted at this outcrop, and no core samples are associated with the Garde abrasion.

The abraded surface of Garde has a relatively homogeneous texture (Figure 3a). It features reflective, light-to-dark gray-green, angular, millimeter-scale mineral grains in a fine-grained light-toned matrix and reflective, dark

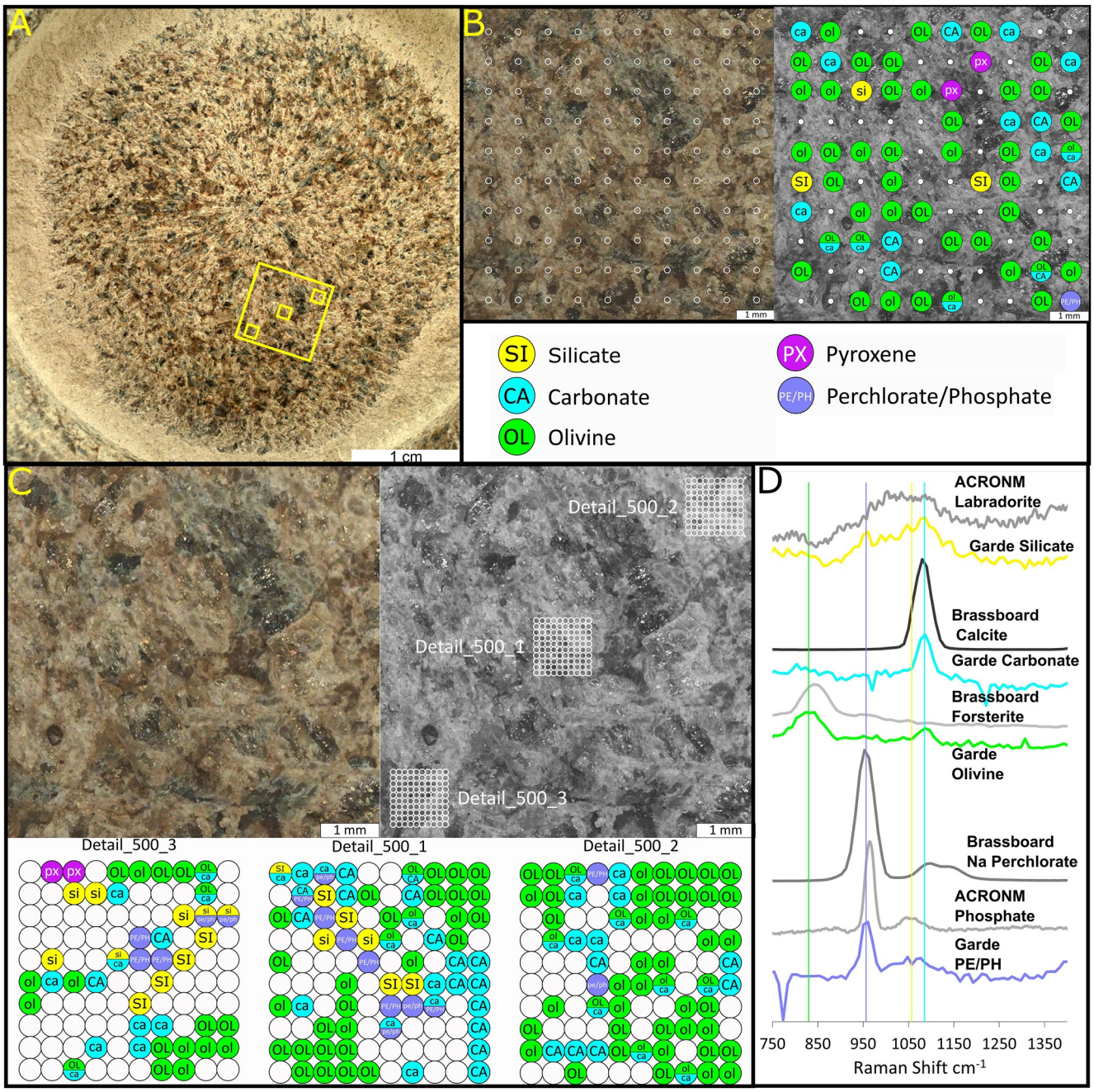

Figure 3. SHERLOC Raman mineral identifications from Garde. (a) The abrasion patch imaged by WATSON (image ID SIF_0206_0685226491_804FDR_N0071836SRLC01024_0000LMJ01). Yellow boxes indicate the location of scans. (b) Colorized (left) and grayscale (right) ACI images (image ID SC3_0208_0685436606_980FDR_N0071836SRLC11372_0000LMJ01) of the region of the abrasion patch bounded by the larger yellow box in panel (a). The white circles in panel B indicate the locations of SHERLOC analysis spots for scan 0207_Garde HDR_500_2. Mineral identifications are indicated in the right panel. (c) Upper Panel: Colorized (left) and grayscale (right) ACI images (image ID SC3_0208_0685432316_968FDR_N0071836SRLC11370_0000LMJ01) of the region of the abrasion patch where the Detail scans occurred. The white circles on the grayscale ACI image in panel C indicate the locations of SHERLOC analysis spots of three 1 mm^2 Detail scans. The lower subpanel shows mineral identifications for the Detail scans. (d) Representative Raman spectra of minerals detected with high confidence and spectra of mineral standards collected on the SHERLOC Brassboard instrument at JPL. Vertical lines indicate peak centers. Spectra are offset along the *y*-axis for clarity.

gray-to-black angular mineral grains that range in size from approximately 1–3 mm across. These are associated with light brown and reddish brown millimeter-scale mineral grains. The surface has no pitting or staining.

SHERLOC scans of Garde include 0207_Garde Survey_15_1, 0207_Garde HDR_500_1, 0207_Garde HDR_500_2, 0208_Garde Detail_500_1, 0208_Garde Detail_500_2, and 0208_Garde Detail_500_3. The Garde survey scan does not contain any spectra with Raman signals strong enough to assign. The remaining scans contain Raman spectra corresponding to olivine, carbonate, silicate, and perchlorate or phosphate, as well as possible pyroxene (Figure 3d).

Olivine was the primary mineral we detected in all of the HDR and Detail scans performed on Garde; 21% of the combined 500 points of these scans were definitively assigned to olivine, and an additional 14% were assigned as probable olivine (Figures 3b and 3c). The dominant peak in the mean spectrum of all points in 0208_Garde Detail_500_1 assigned to olivine is centered at 830 cm^{-1}, represented by the vertical green line in Figure 3d. The points in Garde assigned to olivine generally fall on the reflective gray-green mineral grains.

We also detected carbonate across all of the Garde HDR and Detail scans, with 7% of the 500 points definitively assigned to carbonate and an additional 11% assigned to probable carbonate (Figures 3b and 3c). The dominant peak of the mean spectrum of all points in scan 0208_Garde Detail_500_1 assigned to carbonate is centered at 1085 cm^{-1}, represented by the vertical cyan line in Figure 3d. However, as in the Dourbes carbonate detections, this assignment is to mineral class only and not species. The points assigned to carbonate fall on light brown and reddish brown grains that are closely associated with the olivine grains.

All three of the Garde Detail scans contain Raman spectra that are consistent with perchlorate or phosphate. The dominant peak of the mean spectrum of all points in scan 0208_Garde Detail_500_1 assigned to perchlorate or phosphate is centered at 956 cm^{-1}, represented by the vertical lavender-blue line in Figure 3d. As in Dourbes, this peak falls between the dominant peak of perchlorate and phosphate standards analyzed by SHERLOC analog instruments (see Section 3.1 and Text S4.8 in Supporting Information S1) and cannot be confidently assigned to either mineral. We did not observe hydration features in the Garde spectra assigned to perchlorate/phosphate. The points assigned to perchlorate or phosphate in the Garde Detail scans generally fall on non-reflective light gray grains.

The spectra in scan 0208_Garde Detail_500_1 assigned to perchlorate or phosphate also feature a fluorescence band located at ∼340 nm (Scheller et al., 2022). The ∼340 nm fluorescence feature could result from organic species and/or from trivalent cerium (Ce3+) within a phosphate crystal structure (Shkolyar et al., 2021). The possible presence of (Ce3+) fluorescence may support a phosphate assignment for these spectra. However, the fluorescence spectral assignment is not straightforward (see Text S4.6 in Supporting Information S1).

Scans 0207_Garde HDR_500_2, 0208_Garde Detail_500_1, and 0208_Garde Detail_500_3 contain points assigned to silicate. The silicate detections fall on dark gray non-reflective grains and are often associated with perchlorate or phosphate detections in the Detail scans (Figures 3b and 3c). The mean spectrum of all points in scan 0208_Garde Detail_500_1 assigned to silicate features a broad band centered at 1057 cm^{-1}, represented by the vertical yellow line in Figure 3d. This band is qualitatively similar to one seen in a labradorite spectrum collected by ACRONM (see Text S4.2 in Supporting Information S1) SHERLOC also detected possible pyroxene at six points across 0207_Garde HDR_500_1, 0207_Garde HDR_500_2, and 0208_Garde Detail_500_3. The mean spectrum of these six spectra features a peak at ∼1020 cm^{-1}, which most closely matches the spectrum collected from diopside on Brassboard. However, the comparison to a standard diopside spectrum is not a formal mineral assignment, which will require a detailed investigation beyond the scope of this paper.

3.1.3. Quartier

The Quartier abrasion patch, which was approximately 7 mm deep, was made on sol 292 on Issole, a weathered, tabular outcrop of the Issole member of the Séítah formation, near the contact of the Séítah and Máaz formations (Figure 1). The pre-abrasion surface of Quartier exhibited multiple textures: centimeter-scale platy features, rounded bumps that were up to approximately one cm tall, and a patchy covering of coarse regolith to fine-grained gravel (Figure S2c in Supporting Information S1). It also featured occasional rounded centimeter-scale pebbles. Quartier is associated with two core samples from the Issole outcrop: Robine and Malay (Simon et al., 2022). Abrading Quartier revealed prominent dark gray-to-black angular 1–5 mm mineral grains associated with smaller and less abundant light-to-dark gray minerals that are sometimes rimmed with light reddish-brown material

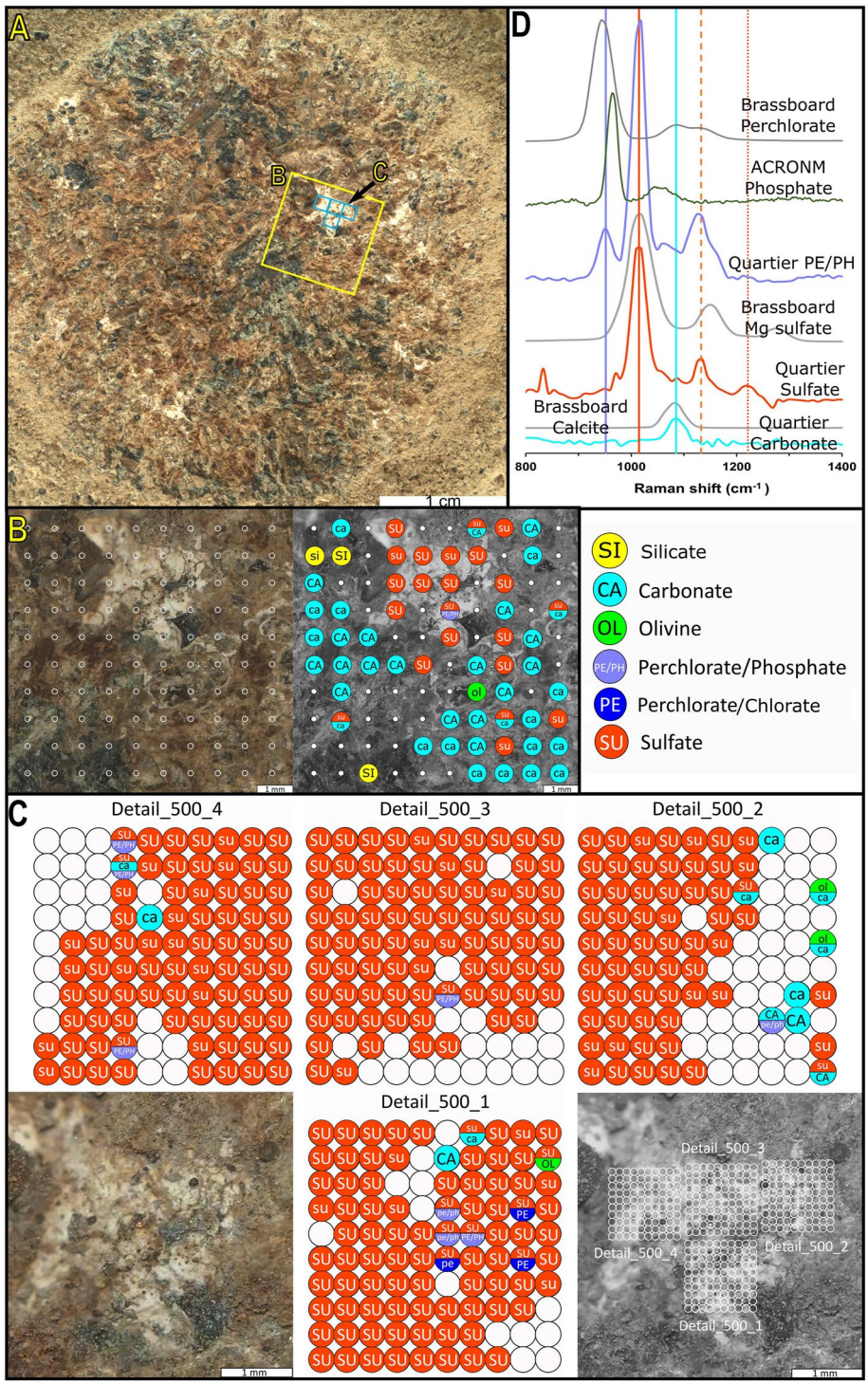

Figure 4. SHERLOC Raman mineral identifications from Quartier. (a) The abrasion patch imaged by WATSON (image ID SIF_0292_0692866773_550FDR_N0090000SRLC00702_0000LMJ01). The yellow box indicates the location of the HDR scan and blue boxes indicate the location of the Detail scans. (b) Colorized (left) and grayscale (right) ACI images (image ID SC3_0293_0692982585_671FDR_N0090000SRLC10600_0000LMJ01) of the region of the abrasion patch bounded by the larger yellow box in panel (a). The white circles in panel B indicate the locations of SHERLOC analysis spots for 0293_Quartier HDR_500_1. Mineral identifications are indicated in the right panel. (c) Colorized (bottom left) and grayscale (bottom right) ACI (image ID SC3_0304_0693962423_667FDR_N0090000SRLC11373_0000LMJ01) images of the region of the abrasion patch where the Detail scans occurred. The white circles on the grayscale ACI image in panel C indicate the locations of SHERLOC analysis spots for four 1 mm^2 Detail scans. The other four subpanels show mineral identifications for Quartier Detail scans. (d) Representative Raman spectra of minerals detected with high confidence from the abrasion patch and spectra of mineral standards collected on the SHERLOC Brassboard instrument at JPL. Vertical lines represent peak centers. Spectra are offset along the *y*-axis for clarity.

(Figure 4a). These gray-to-black mineral grains exist within a light colored matrix. The surface also features scattered, irregularly shaped, bright white mineral grains and closely associated reddish-brown mineral grains. SHERLOC scans of Quartier focused on an area that is dominated by bright white and reddish-brown grains, with some dark gray-to-black grains (Figures 4a and 4b).

SHERLOC scans of Quartier include 0293_Quartier Survey_15_1, 0293_Quartier HDR_500_1, 0304_Quartier Survey_15_1 (which had 50 μm spacing), 0304_Quartier Detail_500_1, 0304_Quartier Detail_500_2, 0304_Quartier Detail_500_3, and 0304_Quartier Detail_500_4 (Figure 4). All of the Quartier scans, including the survey scan, contain spectra that correspond to sulfate. The Quartier HDR and Detail scans also contain spectra corresponding to carbonate, olivine, undefined silicate, perchlorate, and perchlorate or phosphate (Figures 4b–4d).

Carbonate and sulfate were the most abundant minerals detected in 0293_Quartier HDR_500_1 (Figure 4b). Eighteen percent of the points in this scan were definitively assigned to carbonate and an additional 18% were assigned as probable carbonate. The dominant peak of the mean spectrum of all points in 0293_Quartier HDR_500_1 definitively assigned to carbonate, with no second assignment, is centered at 1085 cm^{-1}, represented by the vertical cyan line in Figure 2d. Twelve percent of the points were definitively assigned to sulfate and an additional 9% were assigned as probable sulfate. The mean spectrum of all points in 0293_Quartier HDR_500_1 definitively assigned to sulfate has a primary peak centered at 1011 cm^{-1} and no clear secondary peaks.

The sulfate detections in 0293_Quartier HDR_500_1 are generally collocated with a patch of bright white mineral grains, while the carbonate detections fall on reddish-brown mineral grains surrounding the sulfate grains (Figure 4b). A single point in this scan was assigned as probable olivine. This detection falls on a highly reflective, light gray mineral that is surrounded by carbonate (Figure 4b). The spectrum of one point definitively assigned to sulfate in this scan also contains a peak at 952 cm^{-1} assigned to perchlorate or phosphate. This point falls partially on bright white grains and partially on a small brown grain within the patch of bright white mineral grains (Figure 4b). Two points in the 0293_Quartier HDR_500_1 scan were definitively assigned to silicate and one point was identified as a probable silicate. The silicate detections fall on dark gray-to-black mineral grains (Figure 4b).

The four Quartier Detail scans, which were focused on the bright white mineral grains, are dominated by sulfate detections (Figure 4c). Of the 400 combined points in the Quartier Detail scans, we definitively assigned 66% to sulfate and assigned 11% to probable sulfate. As in the HDR scan of Quartier, the sulfate detections were collocated with the bright white mineral grains. The mean spectrum of all points in 0304_Quartier Detail_500_1 definitively assigned to sulfate only has a primary peak centered at 1015 cm^{-1}, represented by the vertical red line in Figure 4d, and secondary peaks at 1133 cm^{-1} and 1221 cm^{-1}, represented by dashed and dotted vertical red lines, respectively (Figure 4d). The primary peak of the representative Quartier sulfate spectrum and the secondary peak at 1133 cm^{-1} are near the primary and secondary peaks of a gypsum standard (WARDS #46–3798) spectrum collected on Brassboard, which has peaks at 1009 cm^{-1} and 1129 cm^{-1} (Figure 4d). The secondary peak at 1221 cm^{-1} in the Quartier sulfate spectrum does not correspond to any peak in the Brassboard gypsum spectrum. However, the primary peak in the Quartier sulfate spectrum also has good agreement with the primary peak of the synthetic magnesium sulfate (Macron Chemicals) spectrum collected on Brassboard, which is centered at 1019 cm^{-1}, and the two secondary magnesium sulfate peaks that can vary between ∼1060 cm^{-1} and ∼1260 cm^{-1}, according to hydration state (Wang et al., 2006; Figure 4d). The representative Quartier sulfate spectrum has a broad band with two peaks at 3229 cm^{-1} and 3415 cm^{-1}, which is consistent with OH stretching mode bands seen in hydrated sulfates (Figure S10b in Supporting Information S1). Further investigation is needed to establish the primary cation and hydration states of Quartier sulfates at individual points within the Quartier scans, but the mean spectrum presented in Figure 4d and Figure S10b in Supporting Information S1 suggests that the bright white minerals of Quartier is a mixture of calcium and magnesium sulfate at various levels of hydration.

In addition to sulfate, the Quartier Detail scans detected carbonate, olivine, perchlorate/chlorate, and perchlorate or phosphate. Three definitive carbonate detections, one in 0304_Quartier Detail_500_1 and two in 0304_Quartier Detail_500_2, fall on small, reddish-brown mineral grains at the margins of sulfate grains within or at the edge of the bright white patch of sulfate. Only one definitive olivine assignment was made in the Quartier Detail scans. It was at a point that was also definitively assigned to sulfate and falls on small, light gray grains at a boundary between dark gray and bright white grains (Figure 4c). We definitively assigned three points in 0304_Quartier Detail_500_1 to perchlorate or chlorate with unknown cation, all of which were also definitively assigned sulfate. The perchlorate/chlorate assignments were made based on the presence of peaks at 938, 935,

and 931 cm^{-1}, which are consistent with the primary peaks in ACRONM spectra collected from several different oxychlorine species (Figure S12 in Supporting Information S1). The points assigned perchlorate/chlorate fall on light gray-to-brown material at the boundary between a bright white and dark gray-to-black grain (Figure 4c).

We assigned eight points in the Quartier Detail scans to perchlorate or phosphate. Six of these points are also assigned to sulfate, one is also assigned to carbonate, and one is also assigned to both sulfate and carbonate. The perchlorate or phosphate peak in the mean spectrum of the eight perchlorate or phosphate spectra is centered at ~959 cm^{-1} (Figure 4d) and cannot be definitively assigned to perchlorate or phosphate (see Text S4.6 and S4.8 in Supporting Information S1). Most of these detections are associated with hydrated sulfate detections. The single perchlorate/chlorate detection in 0304_Quartier Detail_500_2 that is not associated with sulfate has no discernible hydration features. Like the points assigned perchlorate/chlorate, this point falls on light gray-to-brown material at the boundary of bright white mineral grains.

3.2. Máaz Targets

3.2.1. Guillaumes

Guillaumes was the first abraded patch of the Mars 2020 mission, made on sol 160. This abrasion, which was approximately 8 mm deep, was on a low-relief, polygonal outcrop of the Roubion member of the Máaz formation, also called Roubion (Figure 1). The pre-abrasion surface of the target appeared degraded, granular, and flaky, with regolith embedded in the lowest points and rounded pebbles up to ~5 mm in size across it (Figure S2d in Supporting Information S1). Meter-scale, friable, low-relief, polygonal outcrops are characteristic of the Roubion member, which is at least ~5 m thick and interpreted to be the stratigraphically lowest member of the Máaz formation (Farley et al., 2022). The attempt to core this target produced a borehole and cuttings, but no core was recovered (Simon et al., 2022). The Guillaumes abrasion (Figure 5a) revealed millimeter-scale, interlocking, light and dark mineral grains. Slightly larger, irregularly shaped bright white mineral grains were also present. The abraded surface featured pits and crevices up to approximately 5 mm in diameter. The surface was discontinuously stained dark brown, particularly in and near the pits.

SHERLOC Guillaumes scans included 0161_Guillaumes Survey_15_1, 0161_Guillaumes HDR_100_1, 0161_Guillaumes HDR_100_2, 0161_Guillaumes HDR_300_1, 0162_Guillaumes HDR_250_1 and 0162_Guillaumes HDR_250_2. The sol 161 scans covered an area of the abraded surface that was primarily composed of interlocking light and dark mineral grains with extensive dark brown staining while the sol 162 scans covered an area of interlocking light and dark grains with both irregular bright white mineral grains and discontinuous dark brown staining (Figures S3a–S3c in Supporting Information S1, Figures 5a and 5b).

The sol 161 scans yielded only two spectra with Raman peaks that could be assigned to a mineral class (Figure S3a and S3b in Supporting Information S1). The limited Raman signal observed in this scan may be the result of iron oxide minerals coating much of the area this scan covered, which is suggested by the brown staining on the abraded surface (Figures S3a and S3b in Supporting Information S1, Figure 5a). The two assigned points are point 10 of 0161_Guillaumes HDR_100_2 and point 10 of 0161_Guillaumes HDR_300_1, which are approximately collocated; both are assigned to perchlorate with an unknown cation.

In the sol 162 scans, we observed numerous spectra of sodium perchlorate, perchlorate with no cation assignment, and sulfate, in agreement with Scheller et al. (2022), along with a single possible silicate spectrum (Figure 5 and Figure S3 in Supporting Information S1). The perchlorate and sulfate detections generally fall on irregular bright white mineral grains. The representative Guillaumes sodium perchlorate spectrum in Figure 5c is the mean spectrum of the points in scan 0162_Guillaumes HDR_250_1 assigned to sodium perchlorate with no second assignment (Figure 5b). The dominant peak of this spectrum is centered at 952 cm^{-1}, represented by the vertical solid blue line in Figure 5c. The secondary peaks in this spectrum are centered at 1091 and 1150 cm^{-1}, represented by vertical dashed and vertical dotted blue lines in Figure 5c, respectively. The signal to noise ratios of both the primary and secondary peaks in the individual Guillaumes spectra assigned to sodium perchlorate were greater than 10. For SHERLOC spectra with S/N > 10, the standard deviation of the fitted peak position error is less than 1.2 cm^{-1} (see Text S1 in Supporting Information S1). As a result, we can confidently assign these Guillaumes detections to a specific mineral species. The peaks of the representative Guillaumes sodium perchlorate spectrum directly correspond to the peaks of the sodium perchlorate (Sigma Aldrich 310514) standard spectrum collected on the Brassboard. In addition to peaks at ~950, ~1090, and ~1150 cm^{-1}, the Brassboard spectrum features a

10.1029/2022JE007455

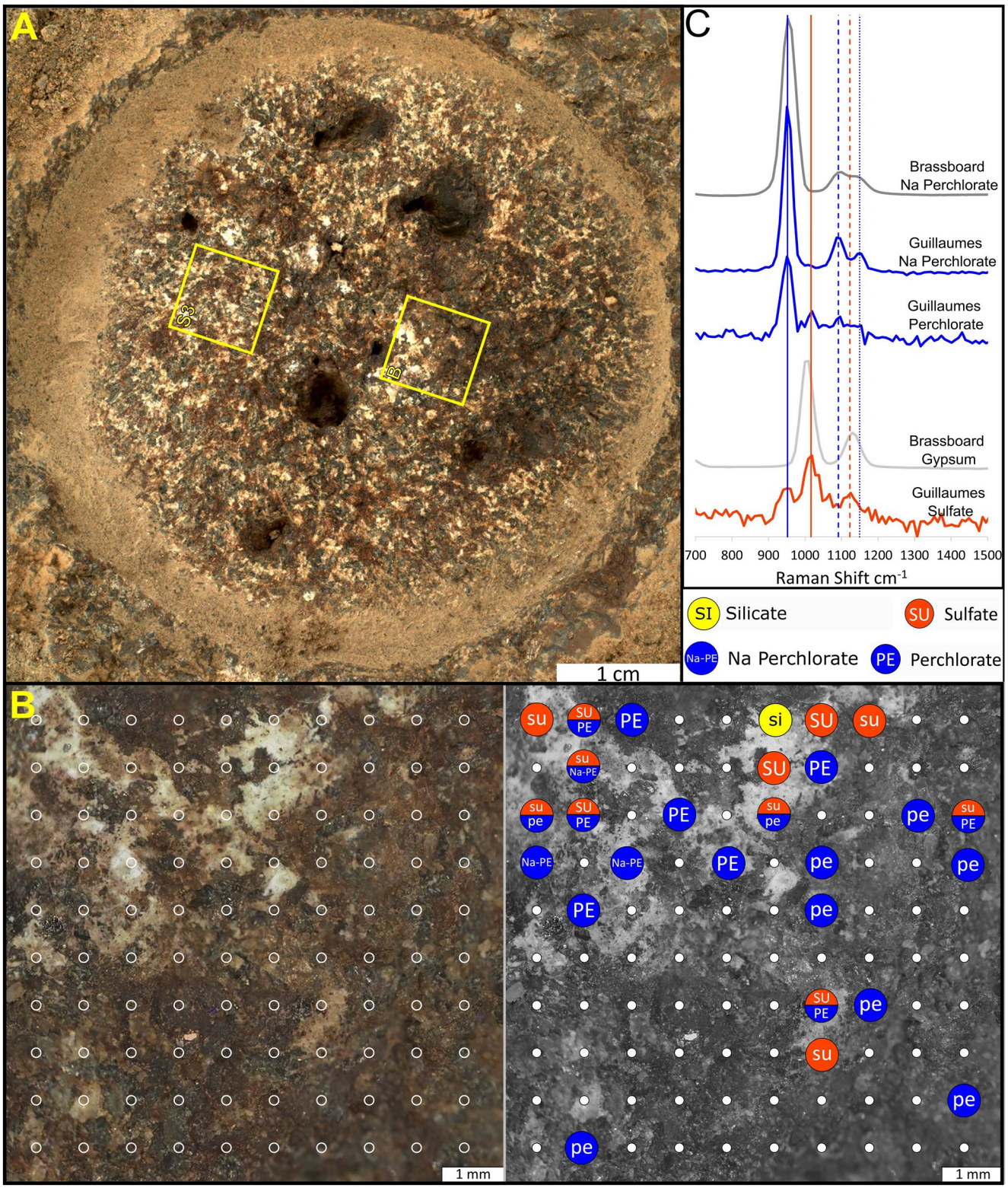

Figure 5.

hydration peak centered at ~3500 cm^{-1} that is approximately three times as intense as the peak at ~1090 cm^{-1}. We did not observe a potential hydration peak in any individual or averaged Guillaumes sodium perchlorate spectra.

The representative Guillaumes perchlorate spectrum in Figure 5c is the mean spectrum of the points in scan 0162_Guillaumes HDR_250_1 definitively assigned to perchlorate with no second assignment (Figure 5b). The dominant peak of this spectrum is centered at 950 cm^{-1}. Secondary peaks were not discernible in individual spectra assigned to perchlorate with unknown cations. However, the mean spectrum displays a weak peak at ~1090 cm^{-1}, which corresponds to the most intense secondary peak in the Brassboard spectrum, and the primary peak corresponds to the primary sodium perchlorate peak, suggesting that the perchlorate spectra represent weak sodium perchlorate detections. This mean spectrum also exhibits a weak peak that corresponds to the primary peak of the sulfate spectra detected in Guillaumes, which demonstrates the close association of perchlorate and sulfate in this target.

The representative Guillaumes sulfate spectrum in Figure 5c is the mean spectrum of the points in scan 0162_Guillaumes HDR_250_1 assigned to sulfate with no second assignment (Figure 5). The dominant peak of this spectrum is centered at 1017 cm^{-1} and the secondary peak is centered at 1123 cm^{-1}, represented by the solid and dashed vertical red lines in Figure 5c, respectively. This spectrum also exhibits a weak, broad OH stretching band with two peaks at 3287 and 3498 cm^{-1}. Similar to the sulfate spectra observed in Quartier scans, peak positions in the representative Guillaumes sulfate spectrum are consistent with some features of several different Brassboard sulfate spectra, including gypsum, epsomite (CVS epsom salts), natural kieserite (JPL mineral collection), and synthetic magnesium sulfate (Macron Chemicals). This suggests that the sulfates detected in Guillaumes may have mixed calcium and magnesium cations, but further investigation is needed before mineral species assignments are made. The mean Guillaumes sulfate spectrum also features a weak peak that corresponds to the primary perchlorate peak, again demonstrating the close association of these two minerals in Guillaumes.

3.2.2. Foux

SHERLOC scanned the natural target Foux on sol 141. SHERLOC also scanned two other natural targets during the Crater Floor Campaign (see Section 3.2.5). Like Guillaumes, Foux was a low-relief, polygonal outcrop of the Roubion member of the Máaz formation. Its surface was somewhat similar to the unabraded surface of Guillaumes. It appeared degraded and had regolith settled into its recesses. It also featured occasional rounded pebbles, up to ~5 mm in size (Figure S2e in Supporting Information S1). The most notable difference between the surface of Foux and the unabraded surface of Guillaumes was the presence of a purplish coating on Foux (Garczynski et al., 2022).

Scans of Foux included 0141_Foux Survey_15_1, 0141_Foux HDR_100_1, 0141_Foux HDR_100_2, and 0141_Foux HDR_300_1. As in the other two natural targets of the Crater Floor Campaign, Nataani and Bi La Sana (see Section 3.2.5), but unlike scans of the abraded targets, the Foux scans produced no single Raman spectra that could be given a mineral assignment. This was expected, as SHERLOC is optimized for analyzing dust-free surfaces with low relief, conditions that were not met on the surface of Foux, Nataani, or Bi la Sana. The median and average spectra of all of the Foux scans showed silicate bands centered between ~1040 cm^{-1} and ~1050 cm^{-1} (Figure S5 in Supporting Information S1) and the fused silica background spectral signature peaks at ~480 and ~800 cm^{-1} discussed in Section 2.4 (Figure S4b in Supporting Information S1).

3.2.3. Montpezat

The Montpezat abrasion, which was approximately 8 mm deep, was made on sol 346 on Rimplas, an outcrop of the Artuby member of the Máaz formation. The surface of Rimplas is coarse-grained and exhibits 1–10 cm thick layers with variable erosion resistance between layers (Figure 1). A coarse-grained surface texture and decimeter thick layers are characteristic of the Artuby member (Farley et al., 2022). The pre-abrasion surface of the

Figure 5. SHERLOC Raman mineral identifications from scan 0162_Guillaumes HDR_250_1. (a) The abrasion patch imaged by WATSON (image ID SI1_0160_0681181210_679FDR_N0060000SRLC00003_000095J01). Yellow boxes indicate the location of the scans performed. The left box corresponds to HDR scans performed on sol 161 (Figure S3 in Supporting Information S1). The right box corresponds to HDR scans performed on sol 162. (b) Colorized (left) and grayscale (right) ACI images (image ID SC3_0162_0681352993_195FDR_N0060000SRLC11420_0000LMJ01) of the region of the abrasion patch bounded by the right yellow box in panel (a). The white circles in panel B indicate the locations of SHERLOC analysis spots. Mineral identifications from scan 0162_Guillaumes HDR_250_1 is indicated in the right panel. (c) Representative Raman spectra of minerals detected with high confidence from the abrasion patch and spectra of mineral standards collected on the SHERLOC Brassboard instrument at JPL. Vertical lines indicate peak centers. Spectra are offset along the *y*-axis for clarity.

10.1029/2022JE007455

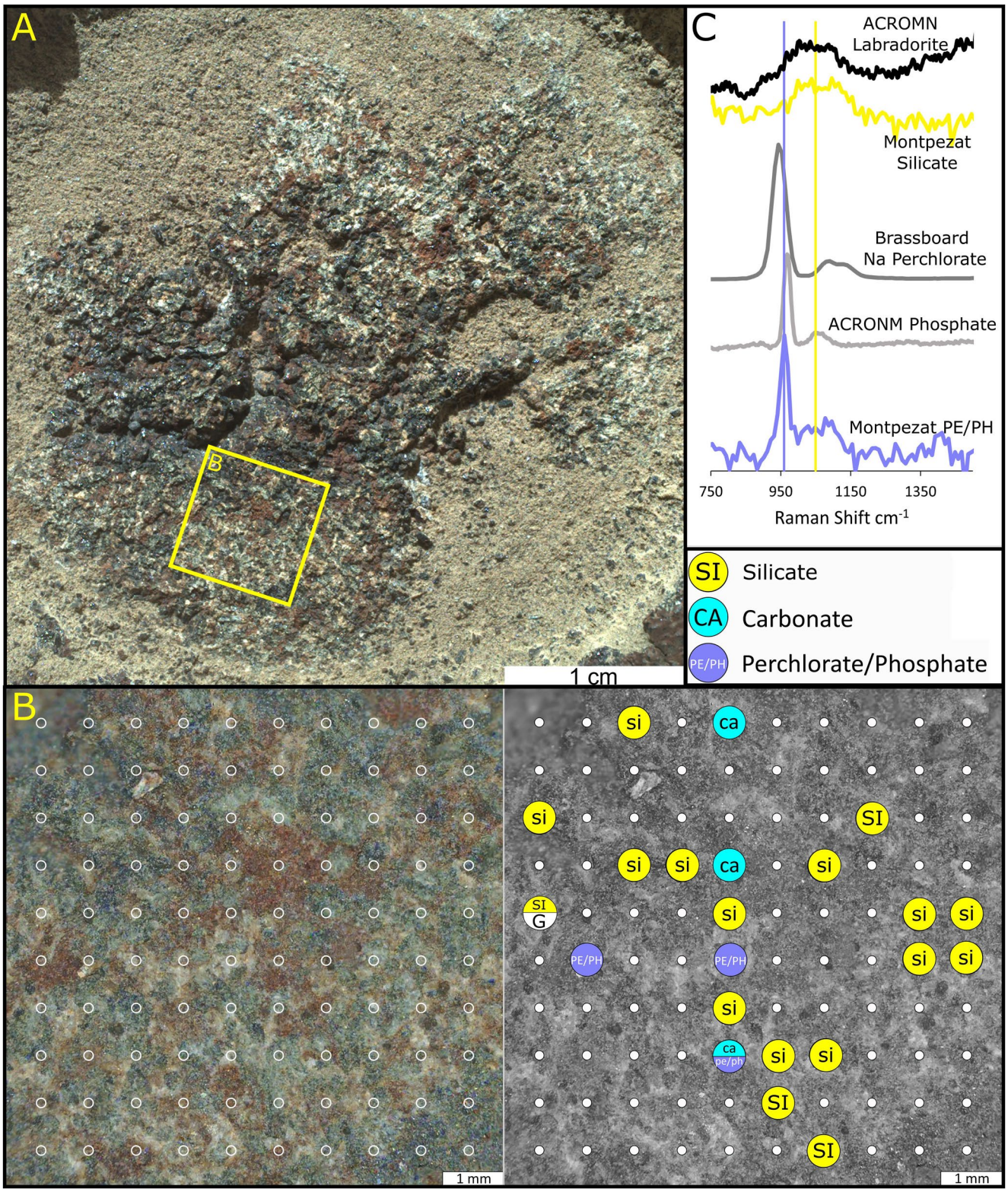

Figure 6. SHERLOC Raman mineral identifications from the 0349_Montpezat HDR_500_1 scan of the target Montpezat. (a) The abrasion patch imaged by WATSON (image ID SIF_0346_0697661461_972FDR_N0092982SRLC01034_0000LMJ01). The yellow box indicates the location of the scan. (b) Colorized (left) and grayscale (right) ACI images (image ID SC3_0349_0697954126_179FDR_N0092982SRLC10600_0000LMJ01) of the region of the abrasion patch bounded by the yellow box in panel (a). The white circles in panel B indicate the locations of SHERLOC analysis spots. Mineral identifications are indicated in the right panel. (c) Representative Raman spectra from the abrasion patch of minerals detected with high confidence, and mineral standard spectra collected on the SHERLOC Brassboard instrument at JPL and the ACRONM instrument at JSC. Spectra are offset along the *y*-axis for clarity.

Montpezat target looked very similar to that of Guillaumes and Foux, with course regolith and fine gravel packed into recesses between bumps up to ~5 mm tall, occasional, rounded, sub-centimeter pebbles, and small patches of purplish coating (Figure S2f in Supporting Information S1). Rimplas was not an intended coring target and the Montpezat abrasion is not associated with any sample cores.

The abraded surface of Montpezat appears highly altered compared to that of the other abraded targets (Figure 6a). It is uneven, perhaps due to pitting that is similar to but more extensive than that seen on Guillaumes. The surface also exhibits extensive staining with dark brown-to-black material. Furthermore, it is partially covered in fine material that is likely cuttings from the abrasion process, possibly because the gDRT used a smaller volume of nitrogen gas to clean Montpezat than it used for previous targets. The least altered or occluded portion of the surface of Montpezat was targeted for SHERLOC scanning, but there was reddish brown staining over much of the scanned surface. The scanned surface exhibits sub-millimeter to millimeter sized interlocking white to dark gray-blue grains.

SHERLOC scans of Montpezat included 0349_Montpezat Survey_15_1 and 0349_ Montpezat HDR_500_1 scans. No points in the Montpezat Survey scan had a discernible Raman signal. The 0394_Montpezat HDR_500_1 scan revealed silicate, carbonate, and perchlorate or phosphate spectral signatures. Seventeen single spectra display silicate signatures; however, only four of those assignments were made with high confidence. We observed three carbonate and three perchlorate or phosphate spectra in the scan. All carbonate spectra and one of the perchlorate or phosphate spectra are of low confidence. Figure 6c shows the mean spectrum of all 0349_Montpezat HDR_500_1 definitively assigned to silicate and the mean spectrum of the two points definitively assigned to perchlorate or phosphate. These peaks are centered at 1050 and 959 cm^{-1} respectively. The Montpezat HDR scan also contains one spectrum with a low, broad band centered at ~1600 cm^{-1}, which may be a graphitic (G) band. The point with the possible G band is indicated by a capital G on a white background in Figure 6b. A report from the SHERLOC team that discusses the context and implications of this detection is forthcoming.

3.2.4. Bellegarde

The Bellegarde abrasion, which was approximately 8 mm deep, was made on sol 185 on a small blocky boulder (approximately 40 cm across; Figure 1) of the Rochette member of the Máaz formation. The boulder was chosen as the second target for abrasion and coring in part because it did not appear to be highly weathered (Figure S2g in Supporting Information S1), indicating a high likelihood for successful core recovery. In fact, the first two successful cores of the Mars 2020 mission, Montdenier and Montagnac, were retrieved from this boulder (Simon et al., 2022). The erosion-resistant Rochette member is approximately 30–50 cm thick and often exhibits centimeter scale layering (Farley et al., 2022). The Rochette member caps the crest of Artuby ridge (Sun et al., 2022).

The abraded surface of Bellegarde (Figure 7a) features sub-millimeter, interlocking, white to dark green-gray mineral grains. We also observed some larger, bright white mineral grains rimmed by a tan material on the surface of Bellegarde. The surface of Bellegarde is partially stained by a reddish-brown material.

SHERLOC scans of Bellegarde include 0186_Bellegarde Survey_15_1, 0186_Bellegarde HDR_250_1, and 0186_Bellegarde HDR_250_2. The data from these scans indicate that Bellegarde contains silicate, perchlorate or phosphate, and sulfate spectral signatures. As reported by Scheller et al. (2022), the Bellegarde Survey scan detected sulfate associated with the largest cluster of bright white minerals in the upper left region of the scan. Only 17 of 200 total spectra across both Bellegarde HDR scans show Raman spectral signatures. The low level of Raman signals in Bellegarde may be due to the presence of iron oxide minerals at the target surface, which is suggested by the reddish-brown staining. Most Bellegarde mineral detections are on regions of the target that has no staining.

The 17 mineral detections in the Bellegarde HDR scans include three definitive and seven probable silicates, which fall on dark gray grains; four probable sulfate, which are only sometimes associated with bright white grains; and two definitive and one probable perchlorate or phosphate, which fall on medium to dark gray grains. Figure 7c shows the mean spectrum of all 0186_Bellegarde HDR_250_2 definitively assigned to silicate and the mean spectrum of the two points definitively assigned to perchlorate or phosphate. These peaks are centered at 1036 cm^{-1} and 955 cm^{-1} respectively. The peak centered at 1036 cm^{-1} is qualitatively similar to the band in a labradorite spectrum collected by ACRONM and assigned silicate (Figure 7c).

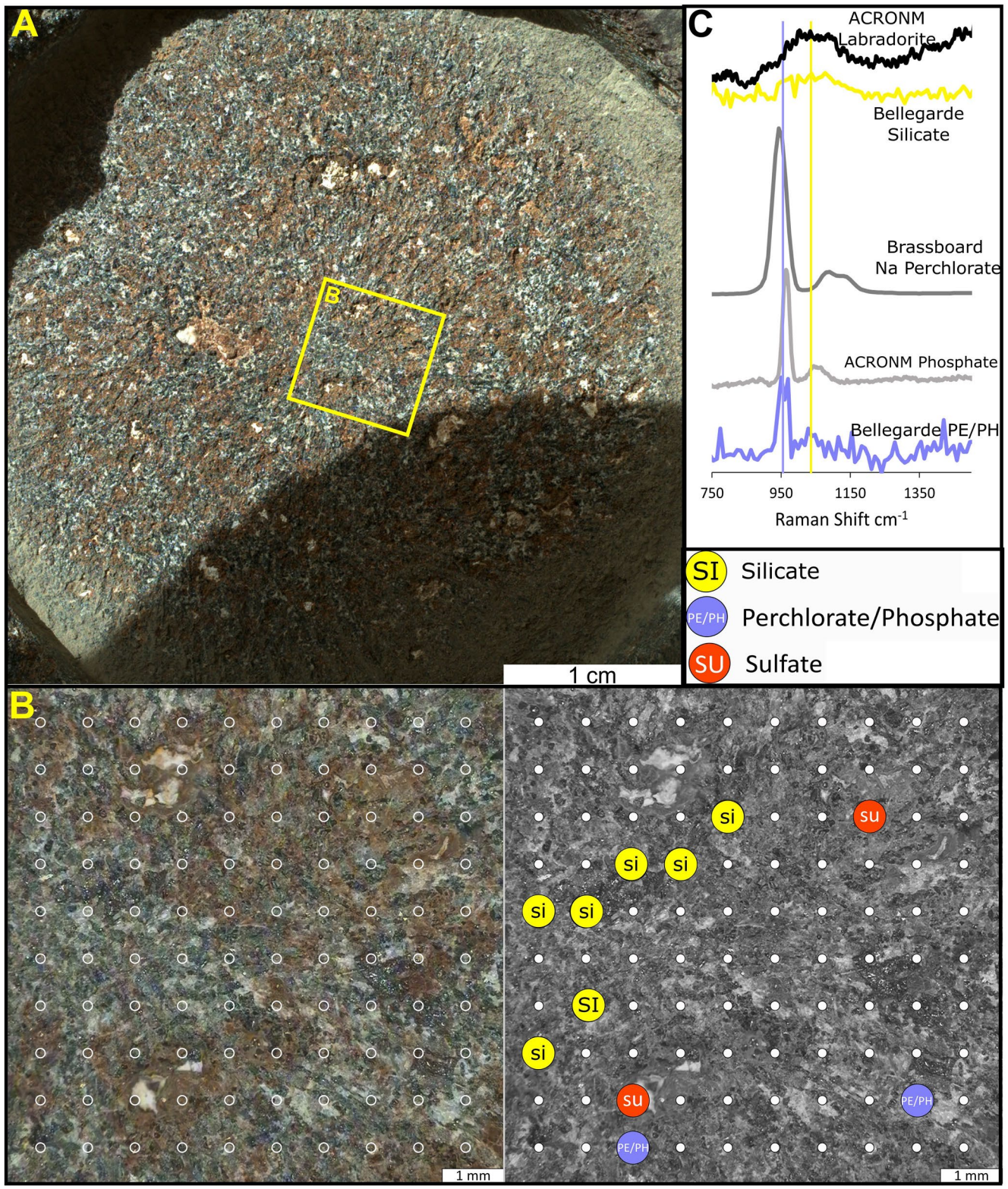

Figure 7. SHERLOC Raman mineral identifications from scan 0186_Bellegarde HDR_250_2 of the target Bellegarde. (a) The abrasion patch imaged by WATSON (image ID SIF_0185_0683368184_652FDR_N0070000SRLC00720_0000LMJ01). The yellow box indicates the location of the HDR. (b) Colorized (left) and grayscale (right) ACI images (image ID SC3_0186_0683479674_054FDR_N0070000SRLC11420_0000LMJ02) of the region of the abrasion patch bounded by the yellow box in panel (a). The white circles in panel B indicate the locations of SHERLOC analysis spots. Mineral identifications are indicated in the right panel. (c) Representative Raman spectra from the abrasion patch of minerals detected with high confidence, and mineral standard spectra collected on the SHERLOC Brassboard instrument at JPL and the ACRONM instrument at JSC. Vertical lines indicate peak centers. Spectra are offset along the *y*-axis for clarity.

As in Garde, the Bellegarde spectra assigned to perchlorate or phosphate also feature a fluorescence band at ~340 nm (Scheller et al., 2022). The ~340 nm fluorescence feature could result from organic species and/or from trivalent cerium (Ce^{3+}) within a phosphate crystal structure (Shkolyar et al., 2021). Therefore, the ~340 nm fluorescence feature may support a phosphate assignment for these detections (see Text S4.6 in Supporting Information S1). Data acquired by Perseverance's SuperCam instrument revealed the presence of an anhydrous sodium perchlorate signature associated with a bright white patch of mineral grains at Bellegarde that was not analyzed by SHERLOC, similar to that detected by both SHERLOC and SuperCam at Guillaumes (see Section 3.2.1; Meslin et al., 2022). Taken together, these analyses suggest the possibility that both phosphate and perchlorate are present in the Bellegarde abrasion.

3.2.5. Nataani and Bi la Sana

SHERLOC's first two sets of scans on Mars were performed on the natural targets Nataani, on sol 83, and Bi la Sana, on sol 98 (Figures S2h and S2i in Supporting Information S1). These targets are expressions of the Nataani member of the Máaz formation, which overlies the Rochette member, according to ground penetrating radar data (Farley et al., 2022).

Scans on Nataani included 0083_Nataani Survey_10_1, which yielded no detectable Raman signal; 0083_Nataani HDR_5_1, which yielded no detectable Raman signal; 0083_Nataani HDR_50_1, which displayed the fused silica background peaks at ~480 and 800 cm^{-1} (see Section 2.4 and Text S2 in Supporting Information S1) in the mean and median spectra; and 0083_Nataani HDR_100_1, which displayed the fused silica background signal and a silicate band centered at ~1055 cm^{-1} in the mean and median spectra (Figure S5 in Supporting Information S1). Unlike most survey scans in the Crater Floor Campaign, which had 144 μm spacing, 0083_Nataani Survey_10_1 had 200 μm spacing.

The sol 98 set of scans of the natural target Bi la Sana included 0098_Bi la Sana Survey_15_1, 0098_Bi la Sana HDR_100_1, 0098_Bi la Sana HDR_100_2, and 0098_Bi la Sana HDR_300_1. All Bi la Sana scans displayed the fused silica background signal and a silicate band centered at ~1050 cm^{-1} in the mean and median spectra (Figure S5 in Supporting Information S1).

While Raman mineral detections were minimal in the natural target scans of the Crater Floor Campaign, compared to the abraded target scans, it is noteworthy that the same silicate signature observed in many abraded target scans also appears in several of the natural target scans.

3.2.6. Alfalfa

The Alfalfa abrasion, which was approximately 9 mm deep, was made on sol 367 on Sid, a boulder in the Ch'aɬ member of the Máaz formation (Figure 1). The Ch'aɬ member overlies the Nataani member (Farley et al., 2022). Sid is a blocky, apparently structureless, gray boulder and a typical representative of the Ch'aɬ member. The light tan-to-gray pre-abrasion surface of Sid was polished and fluted by wind abrasion and relatively dust free (Figure S2j in Supporting Information S1). Two core samples, Ha'ahóni and Atsá, were retrieved from Sid. The Alfalfa abrasion revealed interlocking, sub-millimeter to ~5 mm bright white, brown, gray, and black mineral grains (Figure 8a). The largest of the grains are bright white, lath-like, and highly reflective. There is patchy reddish-brown coloration across the entire abraded surface.

SHERLOC scans of Alfalfa include 0370_Alfalfa Survey_15_1 and 0370_Alfalfa HDR_500_1. The Alfalfa scans contain predominantly silicate spectra with minor components of carbonate and perchlorate or phosphate. In the single HDR Raman scan collected on alfalfa, silicate comprised 44 of the 100 spectra with 30 detections of high confidence. The mean spectrum of the definitive silicate detections contains a broad band centered at 1053 cm^{-1}, which is qualitatively similar to a broad band in a labradorite spectrum collected by ACRONM (Figure 8c). Carbonate and perchlorate or phosphate peaks were found in 5 and 3 spectra respectively. Two of the perchlorate or phosphate assignments were of high confidence and only one of the carbonate assignments was of high confidence. The mean spectrum of the two definitively assigned perchlorate or phosphate detections has a peak centered at 949 cm^{-1} (Figure 8c).

Several of the silicate detections are associated with bright white, highly reflective mineral grains, including a large lathe-like crystal. This mineral morphology suggests that the Alfalfa silicate detections might be plagioclase feldspar minerals. The carbonate detections fall on light brown to red regions of the surface and the perchlorate or phosphate detections appear to fall at the margins of angular, black mineral grains. No mineral detections fell on

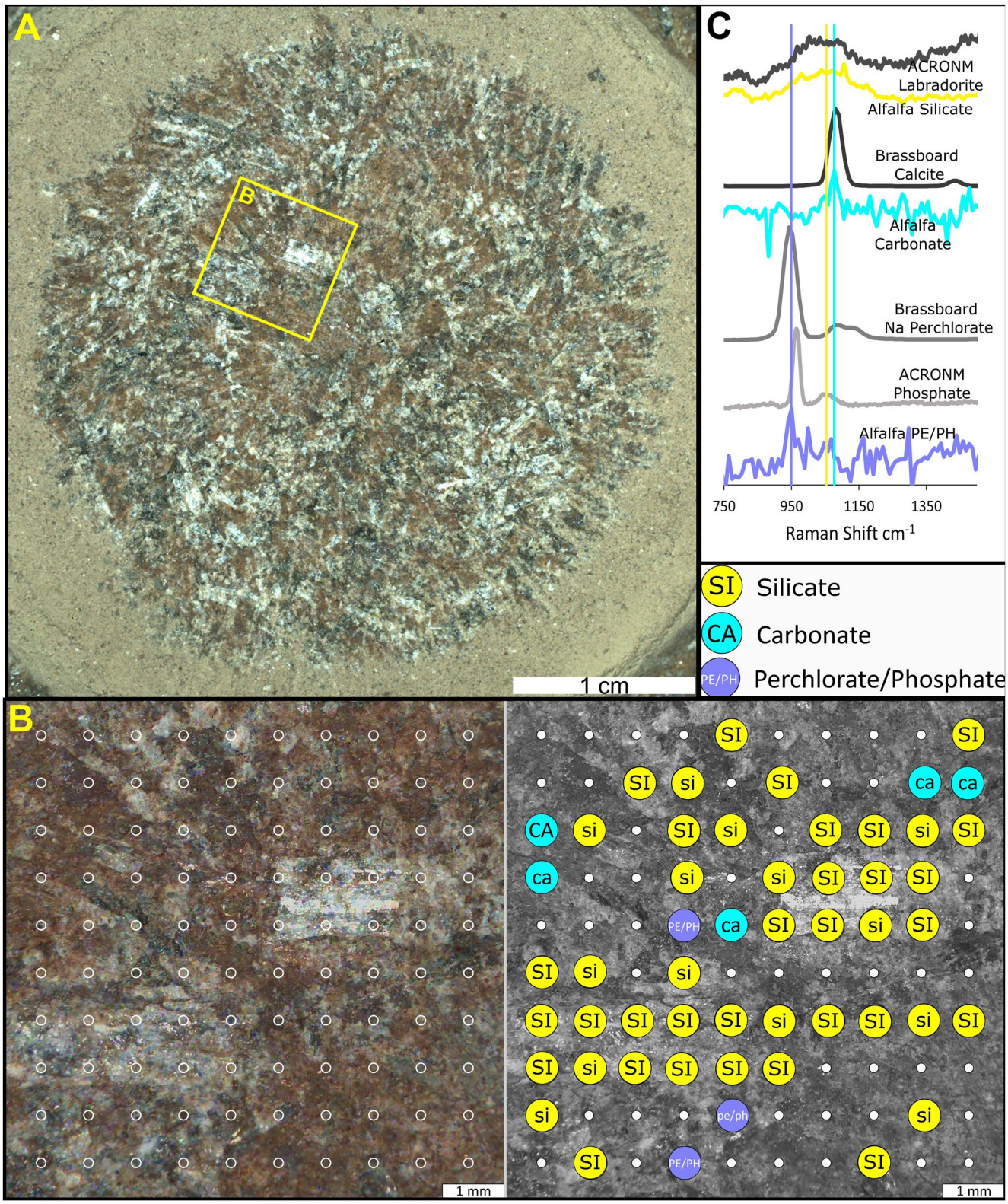

Figure 8.

the reddest regions of the target surface, which may indicate that the red color is the result of the presence of iron cations (Figure 8b), since ferric iron cations can absorb DUV laser radiation (Morris et al., 2022; Razzell Hollis, Abbey, et al., 2021, Razzell Hollis, Ireland, et al., 2021).

4. Discussion

SHERLOC scans of the three abraded Séítah targets and four abraded Máaz targets described above support the conclusions that the Séítah unit is an olivine cumulus and Máaz is a less mafic igneous unit. In addition, the SHERLOC scans reveal that, between them, the Séítah and Máaz units may record the histories of at least three different aqueous alteration events on the floor of Jezero crater, including olivine carbonation and sulfate-dominated salt deposition in Séítah and sodium perchlorate dominated salt deposition in Máaz. The iron oxides present on the four Máaz targets (Wiens et al., 2022) are also likely the result of aqueous alteration. Ultimately, the data acquired by SHERLOC during the Crater Floor Campaign show evidence that Jezero crater was once a chemically active aqueous environment with the potential to host and preserve evidence of microbial life.

Figure 9 shows that the three most common mineral class detections in SHERLOC scans of Séítah targets were olivine, carbonate, and sulfate. Olivine and carbonate detections dominated scans in targets Dourbes and Garde, while minimal olivine was detected in Quartier. Scans of Quartier and Dourbes both revealed patches of sulfate, while Garde scans detected no sulfate. The minimal olivine detections in Quartier and the lack of sulfate detection in Garde may not reflect a major difference in the mineralogy of these targets. The discrepancies may, instead, reflect the SHERLOC team's decision to focus Quartier scans on the bright white patches of the target and the patchy nature of salt deposits in the Séítah formation.

We observe gray grains similar to the one that corresponds to a definitive olivine spectrum in 0304_Quartier Detail_500_1 across the surface of Quartier, sometimes rimmed by light reddish-brown material (Figure 4a). These gray grains appear similar to grains identified as olivine in Dourbes and Garde, and the reddish-brown material looks similar to carbonate that was associated with the olivine in Dourbes and Garde (Figures 2 and 3). While it is possible that Bastide, the outcrop that hosted the Garde abrasion (Figure 1), contains no sulfate deposits, it is equally likely that the Garde abrasion and scans simply did not sample Bastide's sulfate deposits. As demonstrated by the sulfate detected in Dourbes (Figure 2), Séítah sulfate deposits are not all as visually prominent as the sulfate detected in Quartier (Figure 4).

The closely associated olivine and carbonate detections in Garde and Dourbes suggest that the olivine cumulate Séítah unit was exposed to at least one aqueous alteration event, during which partial carbonation of olivine took place (Figures 2 and 3). In particular, detail maps of Dourbes reveal a euhedral olivine crystal with no directly associated carbonate sitting less than one mm away from a subhedral olivine grain with adjacent carbonate grains (Figure 2c). Sulfate deposits in both Dourbes and Quartier are rimmed by carbonate that is both spectrally and morphologically similar to the carbonate associated with olivine in Dourbes and Garde (Figures 2–4). This suggests that all of the carbonates in Séítah formed via the same process, olivine carbonation, and that Séítah's sulfate was deposited later by a sulfate-rich brine in the pore space generated during olivine carbonation through cracking caused by the pressure of carbonate crystal formation (e.g., Xing et al., 2018).

Figure 9 shows that the three most common mineral detections in SHERLOC scans of Máaz targets were silicate, sodium perchlorate, and sulfate. It is important to note the widespread presence of iron oxides in Máaz (Wiens et al., 2022). Iron oxides can absorb deep UV laser radiation and attenuate the spectral signatures of any underlying material (Morris et al., 2022; Razzell Hollis, Abbey, et al., 2021). In all four of the Máaz targets, mineral detections are negatively correlated with the red-to-brown material on their surfaces, which appears consistent with the presence of iron oxide (Figures 5–8). This indicates that SHERLOC's mineral detections in the Máaz formation were limited by the absorption of DUV laser radiation by iron oxide.

Figure 8. SHERLOC Raman mineral identifications from scan 0370_Alfalfa HDR_500_1 of target Alfalfa. (a) The abrasion patch imaged by WATSON (image ID SIF_0367_0699544277_375FDR_N0110108SRLC08029_0000LMJ01). The yellow box indicates the location of the Alfalfa HDR scan. (b) Colorized (left) and grayscale (right) ACI images (image ID SC3_0370_0699816293_742FDR_N0110108SRLC10600_0000LMJ01) of the region of the abrasion patch bounded by the yellow box in panel (a). The white circles in panel B indicate the locations of SHERLOC analysis spots. Mineral identifications are indicated in the right panel. (c) Representative Raman spectra from the abrasion patch of minerals, and mineral standard spectra collected on the SHERLOC Brassboard instrument at JPL and the ACRONM instrument at JSC. Vertical lines indicate peak centers. Spectra are offset along the *y*-axis for clarity.

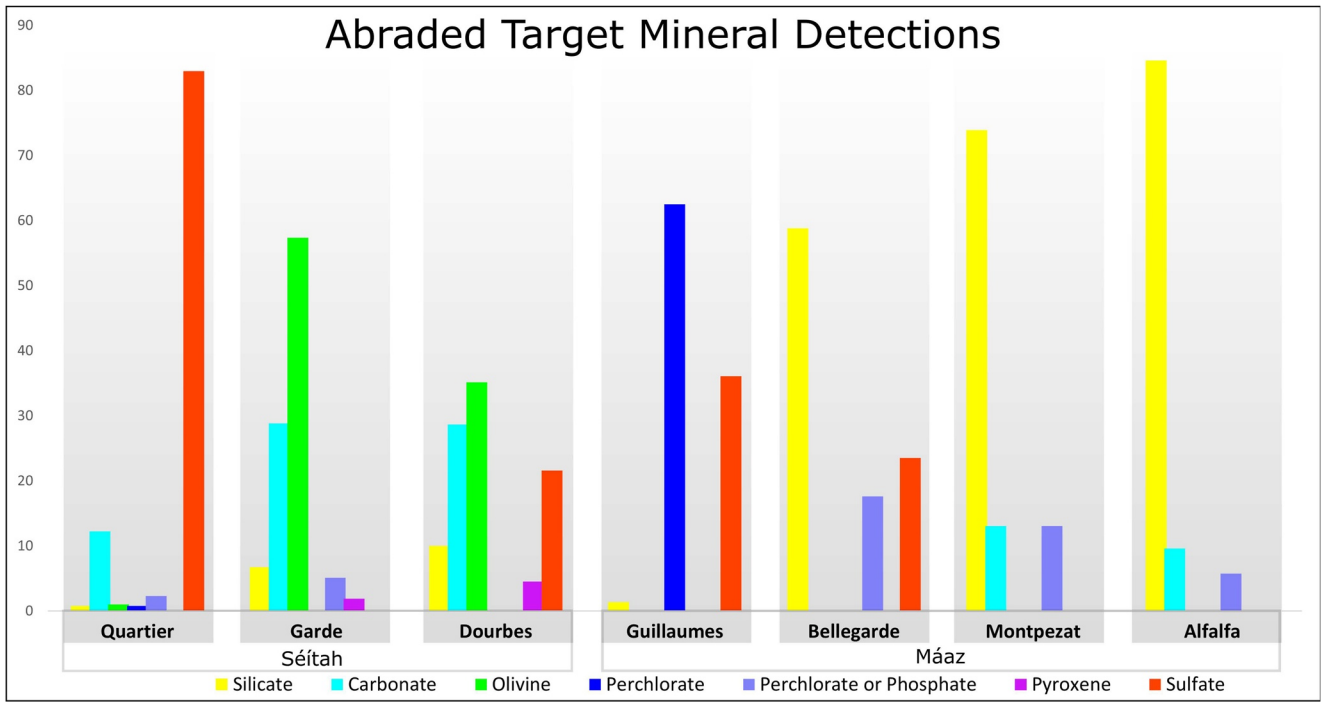

Figure 9. This graph presents, for each abraded target of the Crater Floor Campaign, the percentage of detections of each mineral class out of the total SHERLOC mineral detections per target. Each group of bars associated with each target adds up to 100 percent. Data are presented in this way to correct for the differences in Raman signal intensities between targets discussed in Section 4.1. Séítah formation targets are on the left (Quartier, Garde, and Dourbes) and Máaz targets are on the right (Guillaumes, Bellegarde, Montpezat, and Alfalfa).

Farley et al. (2022) reported that the totality of data collected during the Mars 2020 Crater Floor campaign indicates that the Máaz and Séítah units either originated from two different sources or represent different layers of a single differentiated magma body. The different rock-forming mineral detections of (non-olivine or pyroxene) silicate in the Máaz targets Bellegarde, Montpezat, and Alfalfa, and olivine and pyroxene detections in Séítah targets further support Farley et al.'s interpretation (Figure 9). SHERLOC's microscale mapping of Máaz targets reveals that similar spectra assigned to silicate correspond to grains with very different morphologies. Silicate detections in Montpezat and Bellegarde map to sub-millimeter dark blue-gray grains; in Alfalfa, the detections correspond to mm-scale reflective white lathe-like crystals (Figures 6–8). Although the (non-olivine or pyroxene) silicate spectra reported above were all compared to the same standard labradorite spectrum, the broad bands that led us to assign the spectra to silicate are centered at different wavenumbers: 1050, 1036, and 1053 cm^{-1} in Montpezat, Bellegarde, and Alfalfa, respectively. The variable grain morphology and Raman band placement in Máaz silicate detections suggests that they correspond to at least two different silicate mineral species, and some may actually be amorphous silica detections.

Perchlorate and sulfate detected in Guillaumes and Bellegarde scans are evidence of a third possible aqueous alteration event on the floor of Jezero crater. While the Guillaumes and Bellegarde salt deposits are similar in morphology to the deposits in Dourbes and Quartier, they differ in mineralogy. The deposits in Dourbes and Quartier were predominantly sulfate, with only minor perchlorate contributions (see Sections 3.1.1 and 3.1.3). In contrast, SHERLOC mineral detections on the white patch of minerals in Guillaumes were dominated by perchlorate that can, in some cases, be identified as sodium perchlorate, with lesser, but still significant, sulfate contributions (see Section 3.2.1). SHERLOC scans of Bellegarde detected definitive sulfate signatures alongside perchlorate or phosphate signatures and SuperCam detected a definitive sodium perchlorate signature (Meslin et al., 2022; see Section 3.2.4). Taken together, these SHERLOC and PIXL detections suggest that the salts in Guillaumes and Bellegarde precipitated from a perchlorate-sulfate-bearing brine as it percolated through the Máaz formation rocks.

The mineral detections discussed above are consistent with a changing, habitable aqueous environment that was capable of supporting microbial life and preserving evidence of that life, if it existed. In low-temperature terrestrial

environments, carbonation of mafic to ultramafic rocks, which SHERLOC data from Séítah formation targets indicate occurred in the Jezero crater lake, produces hydrogen that can fuel low-density microbial communities (e.g., Fones et al., 2019; Twing et al., 2017; Woycheese et al., 2015). Terrestrial sulfate and perchlorate brines, similar to the brines that likely deposited the sulfate and perchlorate that SHERLOC detected in Jezero crater, can host microbial life (e.g., Cesur et al., 2022: Fox-Powell & Cockell., 2018; Heinz et al., 2019, 2020). Furthermore, terrestrial sulfate minerals can trap and preserve organic molecules within their structure (e.g., Aubrey et al., 2006; Kotler et al., 2008; Schopf et al., 2012; Shkolyar & Farmer, 2018), and halite- and perchlorate-rich hypersaline subsurface deposits in the Atacama Desert can preserve organic molecules for millions of years (Fernández-Remolar et al., 2013).

5. Conclusions

During the Mars 2020 Crater Floor Campaign, SHERLOC was the first Raman spectrometer to map mineral composition in context on the surface of another planetary body. The microscale mineral maps of abraded Séítah and Máaz targets SHERLOC produced during this campaign reveal differing igneous protoliths with aqueous alteration histories, indicating that the Jezero crater floor was once a habitable aqueous environment and highlight the importance of the proposed Mars Sample Return mission.

SHERLOC data acquired during the Crater Floor Campaign allowed us to identify evidence of olivine carbonation, a process capable of supporting terrestrial microbial metabolic processes (e.g., Fones et al., 2019; Twing et al., 2017; Woycheese et al., 2015), and units bearing sulfate and perchlorate salts, which are known to preserve organic molecules over long periods of time in terrestrial Mars analog environments (Aubrey et al., 2006; Fernández-Remolar et al., 2013; Kotler et al., 2008; Schopf et al., 2012; Shkolyar & Farmer, 2018). These mineral assignments were made with high confidence, and suggest that the return of Crater Floor Campaign samples associated with Dourbes (Salette or Coulettes) and Quartier (Robine or Malay) in Séítah, where we observed evidence of both olivine carbonation and sulfate deposition, and Bellegarde (Montdenier or Montagnac) in Máaz, where we observed evidence of perchlorate and sulfate deposition, could bring preserved evidence of microbial life that may have existed in Jezero crater.

SHERLOC scans performed on the floor of Jezero crater also yielded data that does not allow for straightforward phase assignments, such as the apparent detections of silicate signatures that are common, but associated with differing rock textures, in the Máaz targets Montpezat, Bellegarde, and Alfalfa. The return of Crater Floor Campaign samples associated with Bellegarde (Montdenier or Montagnac) and Alfalfa (Ha'ahóni or Atsá) will allow for laboratory analyses of the sub-millimeter dark blue-gray grains in Bellegarde and large, reflective, lathe-like, white grains in Alfalfa that will provide more definitive, fine scale phase identifications that will facilitate an understanding of the discrepancies in silicate mineral detection between SHERLOC and other Perseverance instruments.

Conflict of Interest

The authors declare no conflicts of interest relevant to this study.

Data Availability Statement

The data used for the study are available on NASA's Planetary Data System (Beegle et al., 2021).

Acknowledgments
We thank the entire Perseverance rover team. The work described in this paper was partially carried out at the Jet Propulsion Laboratory, California Institute of Technology, under a contract with the National Aeronautics and Space Administration. Funding: A.C. was supported by a National Science Foundation Graduate Research Fellowship (award number 2035701). Funding for R.S.J was provided as an Advanced Curation project run by the NASA Astromaterials Acquisition and Curation Office, Johnson Space Center. A.D.C. and A.C. were supported by the Mars 2020 Returned Sample Science Participating Scientist Program (NASA award number 80NSSC20K0237). E.A.C. thanks the Canadian Space Agency (Grant number EXPCOI4) and the Natural Sciences and Engineering Research Council (Grant RGPIN-2021-02995). E.L.S. was supported by NASA Earth and Space Science Fellowship (NESSF) (Grant 80NSSC18K1255) and the SHERLOC Co-I funds of B.L.E. J.R.H. was supported by a NASA Postdoctoral Program fellowship. J.R.H., A.S., L.W.B., R.B., P.G.C., M.F., F.M.M., and A.S.B. were supported by the 107415 Mars 2020 Phase-E. A.J.W. was supported by the NASA M2020 Participating Scientist Program. T.F. was supported by the Italian Space Agency (ASI) Grant agreement ASI/INAF n. 2017-48-H-0. S.S. acknowledges funding from the Swedish National Space Agency (contracts 137/19 and 2021-00092). This work was supported in part by the ISFM Mission Enabling Work Package and the Johnson Space Center.

References

Aubrey, A., Cleaves, H. J., Chalmers, J. H., Skelley, A. M., Mathies, R. A., Grunthaner, F. J., et al. (2006). Sulfate minerals and organic compounds on Mars. *Geology*, *34*(5), 357. https://doi.org/10.1130/G22316.1

Beegle, L. W., Bhartia, R., Deen, R. G., Padgett, D., Algermissen, S., Dunn, A. E., et al. (2021). *Mars 2020 SHERLOC bundle*. NASA Planetary Data System. https://doi.org/10.17189/1522643

Bhartia, R., Beegle, L. W., DeFlores, L., Abbey, W., Razzell Hollis, J., Uckert, K., et al. (2021). Perseverance's scanning habitable environments with Raman and luminescence for organics and chemicals (SHERLOC) investigation. *Space Science Reviews*, *217*(4), 58. https://doi.org/10.1007/s11214-021-00812-z

Bhartia, R., Hug, W. F., & Reid, R. D. (2012). Improved sensing using simultaneous deep UV Raman and fluorescence detection. In *Proceedings of the SPIE 8358, Chemical, Biological, Radiological, Nuclear, and Explosives (CBRNE) Sensing XIII*, 83581A. https://doi.org/10.1117/12.920170

Brown, A. J., Wiens, R. C., Maurice, S., Uckert, K., Tice, M., Flannery, D., et al. (2022). A Komatiite succession as an analog for the olivine bearing rocks at Jezero (abstract). In *Paper presented at the 53rd Lunar and Planetary Science Conference*.

Carrier, B. L., Abbey, W. J., Beegle, L. W., Bhartia, R., & Liu, Y. (2019). Attenuation of ultraviolet radiation in rocks and minerals: Implications for Mars science. *Journal of Geophysical Research: Planets*, *124*(10), 2599–2612. https://doi.org/10.1029/2018JE005758

Cesur, R. M., Ansari, I. M., Chen, F., Clark, B. C., & Schneegurt, M. A. (2022). Bacterial growth in brines formed by the deliquescence of salts relevant to cold arid worlds. *Astrobiology*, *22*(1), 104–115. https://doi.org/10.1089/ast.2020.2336

Chopelas, A. (1991). Single crystal Raman spectra of forsterite, fayalite, and monticellite. *American Mineralogist*, *76*(7–8), 1101–1109.

Edgett, K. S., Yingst, R. A., Ravine, M. A., Caplinger, M. A., Maki, J. N., Ghaemi, F. T., et al. (2012). Curiosity's Mars hand lens imager (MAHLI) investigation. *Space Science Reviews*, *170*(1–4), 259–317. https://doi.org/10.1007/s11214-012-9910-4

Eshelman, E., Daly, M. G., Slater, G., Dietrich, P., & Gravel, J. F. (2014). An ultraviolet Raman wavelength for the in-situ analysis of organic compounds relevant to astrobiology. *Planetary and Space Science*, *93*, 65–70. https://doi.org/10.1016/j.pss.2014.01.021

Farley, K. A., Stack, K. M., Horgan, B. H. N., Tarnas, J., Sun, V. Z., Shuster, D. L., et al. (2022). Aqueously altered igneous rocks on the floor of Jezero crater, Mars. *Science*, *377*(6614), eabo2196. https://doi.org/10.1126/science.abo2196

Farley, K. A., Williford, K. H., Stack, K. M., Bhartia, R., Chen, A., de la Torre, M., et al. (2020). Mars 2020 mission overview. *Space Science Reviews*, *216*(8), 142. https://doi.org/10.1007/s11214-020-00762-y

Fernández-Remolar, D. C., Chong-Díaz, G., Ruíz-Bermejo, M., Harir, M., Schmitt-Kopplin, P., Tziotis, D., et al. (2013). Molecular preservation in halite- and perchlorate-rich hypersaline subsurface deposits in the Salar Grande basin (Atacama Desert, Chile): Implications for the search for molecular biomarkers on Mars. *Journal of Geophysical Research: Biogeosciences*, *118*(2), 922–939. https://doi.org/10.1002/jgrg.20059

Fones, E. M., Colman, D. R., Kraus, E. A., Nothaft, D. B., Poudel, S., Rempfert, K. R., et al. (2019). Physiological adaptations to serpentinization in the Samail Ophiolite, Oman. *The ISME Journal*, *13*(7), 1750–1762. https://doi.org/10.1038/s41396-019-0391-2

Fox-Powell, M. G., & Cockell, C. S. (2018). Building a geochemical view of microbial salt tolerance: Halophilic adaptation of marinococcus in a natural magnesium sulfate brine. *Frontiers in Microbiology*, *9*, 739. https://doi.org/10.3389/fmicb.2018.00739

Fries, M. D., Lee, C., Bhartia, R., Razzell Hollis, J., Beegle, L. W., Uckert, K., et al. (2022). The SHERLOC calibration target on the Mars 2020 Perseverance rover: Design, operations, outreach, and future human exploration functions. *Space Science Reviews*, *218*(6), 46. https://doi.org/10.1007/s11214-022-00907-1

Fu, X., Wang, A., & Krawczynski, M. J. (2017). Characterizing amorphous silicates in extraterrestrial materials: Polymerization effects on Raman and mid-IR spectral features of alkali and alkali Earth silicate glasses: Characterizing amorphous silicates in extraterrestrial materials. *Journal of Geophysical Research: Planets*, *122*(5), 839–855. https://doi.org/10.1002/2016JE005241

Garczynski, B. J., Bell, J. F., Horgan, B. H. N., Johnson, J. R., Rice, M. S., Vaughan, J. I., et al. (2022). Perseverance and the purple coating: A MASTCAM-Z multispectral story (abstract). In *Paper presented at the 53rd Lunar and Planetary Science Conference*.

Heinz, J., Krahn, T., & Schulze-Makuch, D. (2020). A new record for microbial perchlorate tolerance: Fungal growth in $NaClO_4$ brines and its implications for putative life on Mars. *Life*, *10*(5), 53. https://doi.org/10.3390/life10050053

Heinz, J., Waajen, A. C., Airo, A., Alibrandi, A., Schirmack, J., & Schulze-Makuch, D. (2019). Bacterial growth in chloride and perchlorate brines: Halotolerances and salt stress responses of *Planococcus halocryophilus*. *Astrobiology*, *19*(11), 1377–1387. https://doi.org/10.1089/ast.2019.2069

Horgan, B. H. N., Rice, M. S., Garczynski, B. J., Johnson, J. R., Stack, K. M., Vaughan, J. I., et al. (2022). Mineralogy, morphology, and geochronological significance of the Máaz formation and the Jezero Crater Floor (abstract). In *Paper presented at the 53rd Lunar and Planetary Science Conference*.

Kotler, J. M., Hinman, N. W., Yan, B., Stoner, D. L., & Scott, J. R. (2008). Glycine identification in natural jarosites using laser desorption Fourier transform mass Spectrometry: Implications for the search for life on Mars. *Astrobiology*, *8*(2), 253–266. https://doi.org/10.1089/ast.2006.0102

Kuebler, K. E., Jolliff, B. L., Wang, A., & Haskin, L. A. (2006). Extracting olivine (Fo–Fa) compositions from Raman spectral peak positions. *Geochimica et Cosmochimica Acta*, *70*(24), 6201–6222. https://doi.org/10.1016/j.gca.2006.07.035

Lenz, D. D., & Ayres, T. R. (1992). Errors associated with fitting Gaussian Profiles to noisy emission-line spectra. *Publications of the Astronomical Society of the Pacific*, *104*(681), 1104–1106. https://doi.org/10.1086/133096

Liu, Y., Tice, M. M., Schmidt, M. E., Treiman, A. H., Kizovski, T. V., Hurowitz, J. A., et al. (2022). An olivine cumulate outcrop on the floor of Jezero crater, Mars. *Science*, *377*(6614), 1513–1519. https://doi.org/10.1126/science.abo2756

McNaught, A. D., & Wilkinson, A. (1997). *Compendium of chemical terminology*. Blackwell Science.

Meslin, P.-Y., Forni, O., Beck, P., Cousin, A., Beyssac, O., Lopez-Reyes, G., et al. (2022). Evidence for perchlorate and sulfate salts in Jezero crater, Mars, from SuperCam observations (abstract). In *Paper presented at the 53rd Lunar and Planetary Science Conference*.

Moeller, R. C., Jandura, L., Rosette, K., Robinson, M., Samuels, J., Silverman, M., et al. (2021). The Sampling and Caching Subsystem (SCS) for the scientific exploration of Jezero Crater by the Mars 2020 Perseverance rover. *Space Science Reviews*, *217*(1), 5. https://doi.org/10.1007/s11214-020-00783-7

Montagnac, G., Hao, J., Pedreira-Segade, U., & Daniel, I. (2021). Detection of nucleotides adsorbed onto clay by UV resonant Raman spectroscopy: A step towards the search for biosignatures on Mars. *Applied Clay Science*, *200*, 105824. https://doi.org/10.1016/j.clay.2020.105824

Morris, R. V., Haney, N. C., Jakubek, R. S., Fries, M. D., Clark, J. V., Lee, L., & Mertzman, S. A. (2022). Relative detectability of iron-bearing phases for the Mars 2020 SHERLOC deep UV Raman instrument: 1. Focusing on carbonates (abstract). In *Paper presented at the 53rd Lunar and Planetary Science Conference*.

Núñez, J. I., Johnson, J. R., Horgan, B. H. N., Rice, M. S., Vaughan, A., Tate, C., et al. (2022). Stratigraphy and mineralogy of the deposits within Séítah region on the floor of Jezero Crater, Mars as seen with Mastcam-Z (abstract). In *Paper presented at the 53rd Lunar and Planetary Science Conference*.

Razzell Hollis, J., Abbey, W., Beegle, L. W., Bhartia, R., Ehlmann, B. L., Miura, J., et al. (2021). A deep-ultraviolet Raman and Fluorescence spectral library of 62 minerals for the SHERLOC instrument onboard Mars 2020. *Planetary and Space Science*, *209*, 105356. https://doi.org/10.1016/j.pss.2021.105356

Razzell Hollis, J., Ireland, S., Abbey, W., Bhartia, R., & Beegle, L. W. (2021). Deep-ultraviolet Raman spectra of Mars-relevant evaporite minerals under 248.6 nm excitation. *Icarus*, *357*, 114067. https://doi.org/10.1016/j.icarus.2020.114067

Razzell Hollis, J., Moore, K. R., Sharma, S., Beegle, L., Grotzinger, J. P., Allwood, A., et al. (2022). The power of paired proximity science observations: Co-located data from SHERLOC and PIXL on Mars. *Icarus*, *387*(15), 115179. https://doi.org/10.1016/j.icarus.2022.115179

Scheller, E. L., Razzell Hollis, J., Cardarelli, E. L., Steele, A., Beegle, L. W., Bhartia, R., et al. (2022). Aqueous alteration processes and implications for organic geochemistry in Jezero crater, Mars. *Science*, *378*(6624), 1105–1110. https://doi.org/10.1126/science.abo5204

Schmidt, M. E., Allwood, A., Christian, J., Clark, B. C., Flannery, D., Hennecke, J., et al. (2022). Highly differentiated basaltic lavas examined by PIXL in Jezero Crater (abstract). In *Paper presented at the 53rd Lunar and Planetary Science Conference*.

Schopf, J. W., Farmer, J. D., Foster, I. S., Kudryavtsev, A. B., Gallardo, V. A., & Espinoza, C. (2012). Gypsum-permineralized microfossils and their relevance to the search for life on Mars. *Astrobiology*, *12*(7), 619–633. https://doi.org/10.1089/ast.2012.0827

Shkolyar, S., & Farmer, J. D. (2018). Biosignature preservation potential in Playa evaporites: Impacts of diagenesis and implications for Mars exploration. *Astrobiology*, *18*(11), 1460–1478. https://doi.org/10.1089/ast.2018.1849

Shkolyar, S., Lalla, E., Konstantinidis, M., Cote, K., Daly, M. G., & Steele, A. (2021). Detecting Ce^{3+} as a biosignature mimicker using UV time-resolved laser-induced fluorescence and Raman spectroscopy: Implications for planetary missions. *Icarus*, *354*, 114093. https://doi.org/10.1016/j.icarus.2020.114093

Simon, J. I., Amundsen, H. E. F., Beegle, L. W., Bell, J., Benison, K. C., Berger, E. L., et al. (2022). Sampling of Jezero Crater Máaz formation by Mars 2020 Perseverance rover (abstract). In *Paper presented at the 53rd Lunar and Planetary Science Conference*.

Stack, K. M., Williams, N. R., Calef, F., Sun, V. Z., Williford, K. H., Farley, K. A., et al. (2020). Photogeologic map of the Perseverance rover field site in Jezero Crater constructed by the Mars 2020 Science Team. *Space Science Reviews*, *216*(8), 127. https://doi.org/10.1007/s11214-020-00739-x

Sun, V. Z., Hand, K. P., Stack, K. M., Farley, K. A., Milkovich, S., Kronyak, R., et al. (2022). Exploring the Jezero Crater floor: Overview of results from the Mars 2020 Perseverance Rover's first science campaign (abstract). In *53rd Lunar and Planetary Science Conference*.

Tarcea, N., Harz, M., Rösch, P., Frosch, T., Schmitt, M., Thiele, H., et al. (2007). UV Raman spectroscopy—A technique for biological and mineralogical in situ planetary studies. *Spectrochimica Acta Part A: Molecular and Biomolecular Spectroscopy*, *68*(4), 1029–1035. https://doi.org/10.1016/j.saa.2007.06.051

Twing, K. I., Brazelton, W. J., Kubo, M. D. Y., Hyer, A. J., Cardace, D., Hoehler, T. M., et al. (2017). Serpentinization-influenced groundwater harbors extremely low diversity microbial communities adapted to high pH. *Frontiers in Microbiology*, *8*, 308. https://doi.org/10.3389/fmicb.2017.00308

Uckert, K., Bhartia, R., Beegle, L. W., Monacelli, B., Asher, S. A., Burton, A. S., et al. (2021). Calibration of the SHERLOC deep ultraviolet fluorescence–Raman spectrometer on the Perseverance rover. *Applied Spectroscopy*, *75*(7), 763–773. https://doi.org/10.1177/00037028211013368

Udry, A., Sautter, V., Cousin, A., Wiens, R. C., Forni, O., Benzerara, K., et al. (2022). A Mars 2020 Perseverance SuperCam perspective on the igneous nature of the Máaz formation at Jezero crater, Mars (abstract). In *Paper presented at the 53rd Lunar and Planetary Science Conference*.

Wang, A., Freeman, J. J., Jolliff, B. L., & Chou, I.-M. (2006). Sulfates on Mars: A systematic Raman spectroscopic study of hydration states of magnesium sulfates. *Geochimica et Cosmochimica Acta*, *70*(24), 6118–6135. https://doi.org/10.1016/j.gca.2006.05.022

Wiens, R. C., Udry, A., Mangold, N., Beyssac, O., Quantin, C., Sautter, V., et al. (2022). Composition and density stratification observed by SuperCam in the first 300 sols in Jezero Crater (abstract). In *Paper presented at 53rd Lunar and Planetary Science Conference*.

Wojdyr, M. (2010). Fityk: A general-purpose peak fitting program. *Journal of Applied Crystallography*, *43*(5), 1126–1128. https://doi.org/10.1107/S0021889810030499

Woycheese, K. M., Meyer-Dombard, D. R., Cardace, D., Argayosa, A. M., & Arcilla, C. A. (2015). Out of the dark: Transitional subsurface-to-surface microbial diversity in a terrestrial serpentinizing seep (Manleluag, Pangasinan, the Philippines). *Frontiers in Microbiology*, *6*(10), 44. https://doi.org/10.3389/fmicb.2015.00044

Xing, T., Zhu, W., Fusseis, F., & Lisabeth, H. (2018). Generating porosity during olivine carbonation via dissolution channels and expansion cracks. *Solid Earth*, *9*(4), 879–896. https://doi.org/10.5194/se-9-879-2018

References From the Supporting Information

Abbey, W. J., Bhartia, R., Beegle, L. W., DeFlores, L., Paez, V., Sijapati, K., et al. (2017). Deep UV Raman spectroscopy for planetary exploration: The search for in situ organics. *Icarus*, *290*, 201–214. https://doi.org/10.1016/j.icarus.2017.01.039

Adcock, C. T., Hausrath, E. M., Forster, P. M., Tschauner, O., & Sefein, K. J. (2014). Synthesis and characterization of the Mars-relevant phosphate minerals Fe- and Mg-whitlockite and merrillite and a possible mechanism that maintains charge balance during whitlockite to merrillite transformation. *American Mineralogist*, *99*(7), 1221–1232. https://doi.org/10.2138/am.2014.4688

Buzgar, N., & Apopei, A. I. (2009). The Raman study of certain carbonates. *Geologie*, *55*(2). https://doi.org/10.13140/2.1.1358.3368

Buzgar, N., Buzatu, A., & Sanislav, I. V. (2009). The Raman study of certain sulfates. *Analele Stiintifice Ale Universitatii Al. I. Cuza*, *55*, 5–23.

Currie, K. L., Knutson, J., & Temby, P. A. (1992). The Mud Tank carbonatite complex, central Australia-an example of metasomatism at mid-crustal levels. *Contributions to Mineralogy and Petrology*, *109*(3), 326–339. https://doi.org/10.1007/bf00283322

Huang, E., Chen, C. H., Huang, T., Lin, E. H., & Xu, J. (2000). Raman spectroscopic characteristics of Mg-Fe-Ca pyroxenes. *American Mineralogist*, *85*(3–4), 473–479. https://doi.org/10.2138/am-2000-0408

Ishibashi, H., Arakawa, M., Ohi, S., Yamamoto, J., Miyake, A., & Kagi, H. (2008). Relationship between Raman spectral pattern and crystallographic orientation of a rock-forming mineral: A case study of Fo_{89} Fa_{11} olivine. *Journal of Raman Spectroscopy*, *39*(11), 1653–1659. https://doi.org/10.1002/jrs.2094

Lieftink, D. J., Nijland, T. G., & Maijer, C. (1994). The behavior of rare-Earth elements in high-temperature Cl-bearing aqueous fluids; results from the Odegardens Verk natural laboratory. *The Canadian Mineralogist*, *32*(1).

Litasov, K. D., & Podgornykh, N. M. (2017). Raman spectroscopy of various phosphate minerals and occurrence of tuite in the Elga IIE iron meteorite. *Journal of Raman Spectroscopy*, *48*(11), 1518–1527. https://doi.org/10.1002/jrs.5119

Mason, H. E., McCubbin, F. M., Smirnov, A., & Phillips, B. L. (2009). Solid-state NMR and IR spectroscopic investigation of the role of structural water and F in carbonate-rich fluorapatite. *American Mineralogist*, *94*(4), 507–516. https://doi.org/10.2138/am.2009.3095

McCubbin, F. M., Hauri, E. H., Elardo, S. M., Vander Kaaden, K. E., Wang, J., & Shearer, C. K., Jr. (2012). Hydrous melting of the Martian mantle produced both depleted and enriched shergottites. *Geology*, *40*(8), 683–686. https://doi.org/10.1130/g33242.1

McCubbin, F. M., Phillips, B. L., Adcock, C. T., Tait, K. T., Steele, A., Vaughn, J. S., et al. (2018). Discreditation of bobdownsite and the establishment of criteria for the identification of minerals with essential monofluorophosphate (PO_3F^{2-}). *American Mineralogist: Journal of Earth and Planetary Materials*, *103*(8), 1319–1328. https://doi.org/10.2138/am-2018-6440

O'shea, D. C., Bartlett, M. L., & Young, R. A. (1974). Compositional analysis of apatites with laser-Raman spectroscopy: (OH, F, Cl) apatites. *Archives of Oral Biology*, *19*(11), 995–1006. https://doi.org/10.1016/0003-9969(74)90086-7

Sudarsanan, K. T., & Young, R. A. (1969). Significant precision in crystal structural details. Holly Springs hydroxyapatite. *Acta Crystallographica Section B*, *25*(8), 1534–1543. https://doi.org/10.1107/s0567740869004298

Walrafen, G. E., & Krishnan, P. N. (1981). Raman spectrum of pressure compacted fused silica. *The Journal of Chemical Physics*, *74*(9), 5328–5330. https://doi.org/10.1063/1.441703

Zapata, F., & Garcia-Ruiz, C. (2018). The discrimination of 72 nitrate, chlorate and perchlorate salts using IR and Raman spectroscopy. *Spectrochimica Acta*, *189*, 535–542. https://doi.org/10.1016/j.saa.2017.08.058